

Eberhard Karls University Tübingen
Geography

Swiss National Park
Research and Geoinformatics

Structure from Motion in an alpine environment –

evaluation of the method and assessment of channel topography change on
the example of the mountain stream Ova dal Fuorn
(Swiss National Park, SNP)

In partial fulfillment of the requirements for the Degree of
Master of Science Geography

Submitted by: Daniel Thiex
Student number: 4095529
E-Mail: daniel.thiex@gmail.com

Supervisor: Dr. Steffen Seitz (Eberhard Karls University Tübingen)
Co-Supervisor: Dr. Samuel Wiesmann (Swiss National Park)

Tübingen, May 2019

Contents

List of Figures	iii
List of Tables	v
List of Acronyms	vii
Abstract/Zusammenfassung	ix
1 Introduction	1
2 Methods	5
2.1 Study area	5
2.2 Data acquisition	7
2.2.1 DTM from LiDAR	7
2.2.2 Aerial photos	7
2.2.3 Ground Control Points	8
2.3 Processing	12
2.3.1 Pix4Dmapper and PhotoScan	12
2.3.2 DTMs from aerial photos using SfM-MVS	13
2.3.3 DTMs of Difference	15
2.4 Validation	16
2.4.1 Software comparison	16
2.4.2 Error metrics	17
2.4.3 DoDs detection threshold	18
3 Results	21
3.1 Pix4Dmapper versus PhotoScan	21
3.1.1 Software properties and settings	21
3.1.2 Processing time	23
3.1.3 Model quality	24
3.1.4 Software pricing	26
3.2 DTMs from aerial photos using SfM-MVS	27
3.3 Change analysis 2003–2018	31
4 Discussion	35
4.1 Pix4Dmapper versus PhotoScan	35
4.1.1 Software properties and settings	35
4.1.2 Processing time	36
4.1.3 Model quality	37

4.1.4	Software pricing	39
4.2	DTMs from aerial photos using SfM-MVS	40
4.3	Change analysis 2003–2018	42
5	Conclusion	45
5.1	Implications	45
5.2	Prospective	47
6	References	49
	Appendix	57

List of Figures

1	Confluence <i>Ova da Val Ftur/Ova dal Fuorn</i>	5
2	Climate chart Buffalora, long-term average 1980–2010	6
3	Exemplary GCP within the study object	9
4	GCPs of the all scenario (A)	11
5	GCPs of the half uniform scenario (B)	11
6	GCPs of the half tmb scenario (C)	11
7	GCPs of the quarter tmb scenario (D)	11
8	Workflow with all processing tasks executed in Pix4Dmapper and PhotoScan	14
9	Point Cloud Classification in Pix4Dmapper	22
10	Point Cloud Classification in PhotoScan	23
11	DTM from SfM-MVS created with Pix4Dmapper, 7.6 cm pixel resolution, all scenario	28
12	DTM from SfM-MVS created with PhotoScan, 2.97 cm pixel resolution, all scenario	29
13	DoD PhotoScan-Pix4Dmapper (top) and 2 enlarged extracts (bottom-left) with corresponding orthofoto (bottom-right)	30
14	Histogramm of the DoD PhotoScan-Pix4Dmapper	31
15	DoD 2009-2003 (top) and four enlarged extracts (bottom), 2 m resolution .	33
16	DoD 2018-2009 (top) and four enlarged extracts (bottom), 1 m resolution .	34

List of Tables

1	Specifications Falcon 8	8
2	Comparison of noticeable software properties	21
3	Processing times (hh:mm:ss) for both programmes	24
4	RMSE [m] of the georeferencing GCPs	24
5	MAE [m] of the georeferencing GCPs	25
6	RMSE [m] for the 21 validation points	25
7	MAE [m] for the 21 validation points	25
8	RMSE _{xyz} [m] and MAE _{xyz} [m] for the georeferencing points and for the validation points	26
9	Pricing and system requirements for Pix4Dmapper and PhotoScan	27
10	Volumetric changes [m ³] between 2003 and 2009 for the single sections and in total	31
11	Volumetric changes [m ³] between 2009 and 2018 for the single sections and in total	32

List of Acronyms

DEM	Digital Elevation Model
DGPS	Differential Global Positioning System
DoD	DTM of difference
DT	Detection Threshold
DTM	Digital Terrain Model
GCP	Ground Control Point
GIS	Geographic Information System
GPS	Global Positioning System
GSD	Ground Sample Distance
LiDAR	Light Detection and Ranging
MAE	Mean Absolute Error
MAD	Mean Absolute Deviation
ME	Mean Error
MVS	Multi-View Stereo
RMSE	Root Mean Square Error
RTK	Real Time Kinematic
SfM	Structure from Motion
SfM-MVS	Structure from Motion-Multi-View Stereo
SIFT	Scale-invariant feature transform
SNP	Swiss National Park

Abstract

Keywords: Pix4Dmapper, PhotoScan, Change detection, Georeferencing, Accuracy evaluation.

In the last years Digital Terrain Models (DTMs) created with Structure from Motion-Multi-View Stereo (SfM-MVS) have been widely used in the field of geomorphology. So far, little attention has been paid to the distribution and number of Ground Control Points (GCPs) for georeferencing the model in a longish research area. Therefore, the aim of this study is to test three different distributions and three different numbers of GCPs using two commercial software programmes (Agisoft PhotoScan and Pix4Dmapper) in a mountain stream environment (*Ova dal Fuorn*) in Switzerland. For the evaluation of the GCP settings, DTMs of Difference (DoDs) and two error metrics (Root Mean Square Error (RMSE) and Mean Absolute Error (MAE)) were deployed. For the software comparison a number of aspects have been taken into account, namely the user friendliness, the processing time, the model quality and the software pricing. It was found that the best model quality is achieved when using the highest number of GCPs—in this case 42—spread equally over the study area. Here for both programmes a low RMSE of 0.05 m and a low MAE of 0.03 m for Pix4Dmapper and 0.04 m for PhotoScan could be reached. The software comparison showed that neither software is clearly superior over the other. Pix4Dmapper is slightly better in terms of accuracy and user-friendliness, whereas PhotoScan runs more stable while processing and has a more attractive pricing system, especially for research.

One field where SfM-MVS DTMs are used is for geomorphic change detection. Due to a heavy thunderstorm in the summer of 2017 the stream bed of the *Ova dal Fuorn* experienced severe changes. Therefore, in a second step the best created DTM was compared via a DoD with a Light Detection and Ranging (LiDAR) DTM from the year 2009 to detect and quantify the changes. To be able to classify the changes and to be able to take a look at the temporal development, the 2009 DTM was compared with a LiDAR DTMs from 2003. Via the DoDs, the areas where changes occurred were located and their

volume in cubic metre was calculated. The results showed that the changes between 2009 and 2018 were more severe than between 2003 and 2009 and can most likely be linked to the 2017 event.

Zusammenfassung

Schlagworte: Pix4Dmapper, PhotoScan, Veränderungsanalyse, Georeferenzierung, Genauigkeitsanalyse.

In letzter Zeit werden immer häufiger mit SfM-MVS erstellte digitale Geländemodelle (DGMs) zur Beantwortung von geomorphologischen Fragestellungen genutzt. Dabei wurde bisher selten die Anzahl und Verteilung von GCPs zur Georeferenzierung des Modelles in einem länglichen Untersuchungsgebiet genauer untersucht. Das Ziel dieser Arbeit ist es daher, drei unterschiedliche Zahlen und drei Verteilungen von GCPs mithilfe von zwei kommerziellen Programmen (Agisoft PhotoScan und Pix4Dmapper) in einem Bergfluss in der Schweiz (*Ova dal Fuorn*) zu vergleichen. Zur Evaluierung der unterschiedlichen GCP Zusammenstellungen wurden ein DoD und zwei Fehlermaße (RMSE und MAE) herangezogen. Für den Vergleich der zwei Programme wurden mehrere Aspekte einbezogen, nämlich die Nutzerfreundlichkeit, die Prozessierungszeit, die spätere Modellqualität und die Anschaffungskosten. Es konnte gezeigt werden, dass die beste Modellqualität bei einer hohen Anzahl – in diesem Fall 42 – und gleichmäßiger Verteilung von GCPs erreicht werden kann. Für diesen Fall konnte ein kleiner RMSE von 0.05 m für beide Programme erreicht werden und ein MAE von 0.03 m für Pix4Dmapper und 0.04 m für PhotoScan. Der Vergleich der zwei Programme hat gezeigt, dass keines dem anderen deutlich überlegen ist. Pix4Dmapper hat leicht bessere Werte in der Modellgenauigkeit, PhotoScan läuft dafür stabiler und bietet attraktivere Preise, vor allem für die Forschung.

Ein Einsatzfeld, in dem DGMs aus SfM-MVS genutzt werden, ist die Untersuchung von geomorphologischen Veränderungen. Als Folge eines schweren Unwetters im Sommer 2017 kam es im Flussbett des *Ova dal Fuorn* zu größeren Veränderungen. Daher wurde in einem zweiten Schritt das beste erstellte DGM herangezogen und mit einem LiDAR DGM von 2009 verglichen, um die Veränderungen festzustellen und quantifizieren zu können. Um die Veränderungen einordnen und die zeitliche Entwicklung besser nachvollziehen zu können,

wurde das 2009 DGM mit einem weiteren LiDAR DGM aus dem Jahr 2003 verglichen. Mithilfe der DoDs konnten die Bereiche, in denen es zu Veränderungen kam, lokalisiert werden und ihr Volumen in Kubikmeter ließ sich berechnen. Als Ergebnis zeigte sich, dass die Veränderungen zwischen 2009 und 2018 deutlich größer waren als die zwischen 2003 und 2009 und am wahrscheinlichsten auf das Unwetter 2017 zurückzuführen sind.

1 Introduction

In the light of climate change it is most likely that geomorphologically damaging events (e.g. flash floods or debris flows) will be more frequent and more severe (Harb et al., 2013). To reach a better understanding of earth surface processes like those mentioned but also in general, multi-time high resolution Digital Terrain Models (DTMs) can play a major role (Chandler et al., 2002; Mali and Kuiry, 2018). In recent years more and more studies have used therefore DTMs created with the method Structure from Motion-Multi-View Stereo (SfM-MVS) out of areal photos (cf. Agüera-Vega et al., 2017; Dietrich, 2016; van Iersel et al., 2018) and especially physical geographers have been quick in implementing SfM-MVS (Smith et al., 2016). SfM-MVS is a inexpensive, non-time-consuming photogrammetric method, which requires little expertise compared to other methods that procure DTMs (Smith et al., 2016).

Although the workflow has a high degree of automation (Mancini et al., 2013), a lot of parameters can be modified influencing the results. So far the default options are neither often changed, nor if changed reported (Smith et al., 2016). One particularly important parameter is the number and distribution of Ground Control Points (GCPs) used when georeferencing the model (Martínez-Carricondo et al., 2018). Initial research in this domain was for example done by Tahar (2013), who found that for equally distributed GCPs the best results were reached with the highest number of GCPs (in this case eight and nine). More recent works were carried out by Agüera-Vega et al. (2017) or Martínez-Carricondo et al. (2018). The first mentioned tested nine different amounts of GCPs (between 4 and 20) each in five different arrangements. They came to the result that 15 GCPs lead to the same results as 20 GCPs in terms of accuracy and therefore preferred 15 over 20 to save time during the acquisition. The latter mentioned found that for between 4 and 36 GCPs in different distributions best results – up to a certain amount of GCPs – are reached when using a higher number and when placing them at the edges but also inside the study area. The few works that investigated the amount and distribution of GCPs so far including the ones mentioned, however deal with a relatively squared research area, a shape rarely found when investigating rivers/streams in narrow mountain valleys.

In addition to the broad range of settings available, there is a number of commercial and non-commercial software to process the SfM-MVS workflow (Carrivick et al., 2016). Whereas some studies compare the performance of non-commercial approaches among themselves (Stumpf et al., 2015; Micheletti et al., 2015) or between commercial and non-commercial software (Jaud et al., 2016; Mali and Kuiry, 2018; Ouédraogo et al., 2014), few research has been conducted on a comparison between two commercial software programmes. To reduce the uncertainty concerning the ideal GCP setting for the investigation of rivers/streams in narrow mountain valleys and concerning the question which commercial software to use, two hypotheses will be tested:

Hypothesis 1:

Due to its widely use in geomorphology (Cook, 2017) it is assumed that Agisoft's software PhotoScan is superior over the software Pix4Dmapper when taking the pricing, the user friendliness and the performance into account.

Hypothesis 2:

Transferred from a squared to a longish research area best results are obtained when placing the GCPs at the edges and inside the study area and when a higher number of GCPs are used.

One surface process where DTMs of rivers/streams are used is the investigation of channel topography changes (cf. Blason et al., 2014; Rascher and Sass, 2017). Detailed knowledge about the channel topography is not only important from an ecological perspective as the topography is important for the habitats (Lane, 2000), but identifying the magnitude and structure behind changes also helps to understand the underlying drivers and processes (James and Robson, 2012). Major changes can often be observed after severe rainfall events (Sass et al., 2015). One big event – a heavy thunderstorm – took place in the Swiss National Park (SNP) in 2017 when during three days 70 per cent of the long-term average precipitation for June, respectively 61.4 mm, were recorded (28–30.06.2017) (ENPK, 2017, MeteoSchweiz (2018a)). During the event a bridge crossing the *Ova val dal Ftur* was flushed away and the small tributary dammed the bigger *Ova dal Fuorn* at its confluence (ENPK, 2017). So far the changes in the streambed of the *Ova dal Fuorn* triggered by the thunderstorm have been granted little attention and have not been closer investigated. Hence, in a second step the by this work created DTM is compared with a Light Detection and Ranging (LiDAR) DTM from 2009 and one from 2003 with 2009 to access the changes in the streambed topography in the period 2003–2018. The two hypotheses will be verified.

Hypothesis 3:

The 2017 event had a major impact on the channel topography of the *Ova dal Fuorn* and thus changes during the period 2009–2018 are more severe than during 2003–2009.

Hypothesis 4:

DTMs derived from SfM-MVS can be used to perform change detection analyses.

To answer the four presented hypotheses, aerial photos of a mountain stream in Switzerland were taken and with different GCP settings in PhotoScan as well as in Pix4Dmapper processed into two DTMs. For this purpose both programmes use the method SfM-MVS and it was evaluated how well both perform. With the resulting DTM and earlier DTMs of the region, the change in time was calculated by subtracting the DTMs from each other. The found changes were finally analysed and tried to be connected to the 2017 rainfall event.

2 Methods

2.1 Study area

The study area is a 2 km long section of the mountain stream *Ova dal Furon* in the SNP in the east of Switzerland's Canton of Grisons. The investigated section lies between the Hotel Il Fuorn (1790 m a.s.l., EPSG 2056: 2'812'087, 1'171'849) and the customs station Punt dal Gall (1700 m a.s.l. EPSG 2056: 2'810'540, 1'170'669). Hence, the stream overcomes in the section a vertical distance of 90 m and around halfway the *Ova da Val Ftur* enters (cf. figure 1).



Figure 1: Confluence *Ova da Val Ftur/Ova dal Fuorn* (photo taken by Daniel Thiex)

The *Ova dal Furon* is a small near-natural mountain stream with a total length of about 14 km and a catchment area of 57.6 km² (geo.admin.ch, 2019). The main type of rock found within the catchment is dolomite (Haller et al., 2014), which provides the *Ova dal Fuorn* with a lot of sediment because of its brittle structure (Rascher and Sass, 2017). The climate in the area – measured at the nearest climate station *Buffalora* 5 km further upstream on 1968 m a.s.l. – is characterized by cold winters (mean temperature in January -9.2°C) when most of the precipitation comes as snow and relatively wet summers (around 300 mm between June and August) (cf. figure 2). The annual average mean temperature

for the reference period 1980–2010 is 0.7°C and the annual mean precipitation 793 mm (MeteoSchweiz, 2018b).

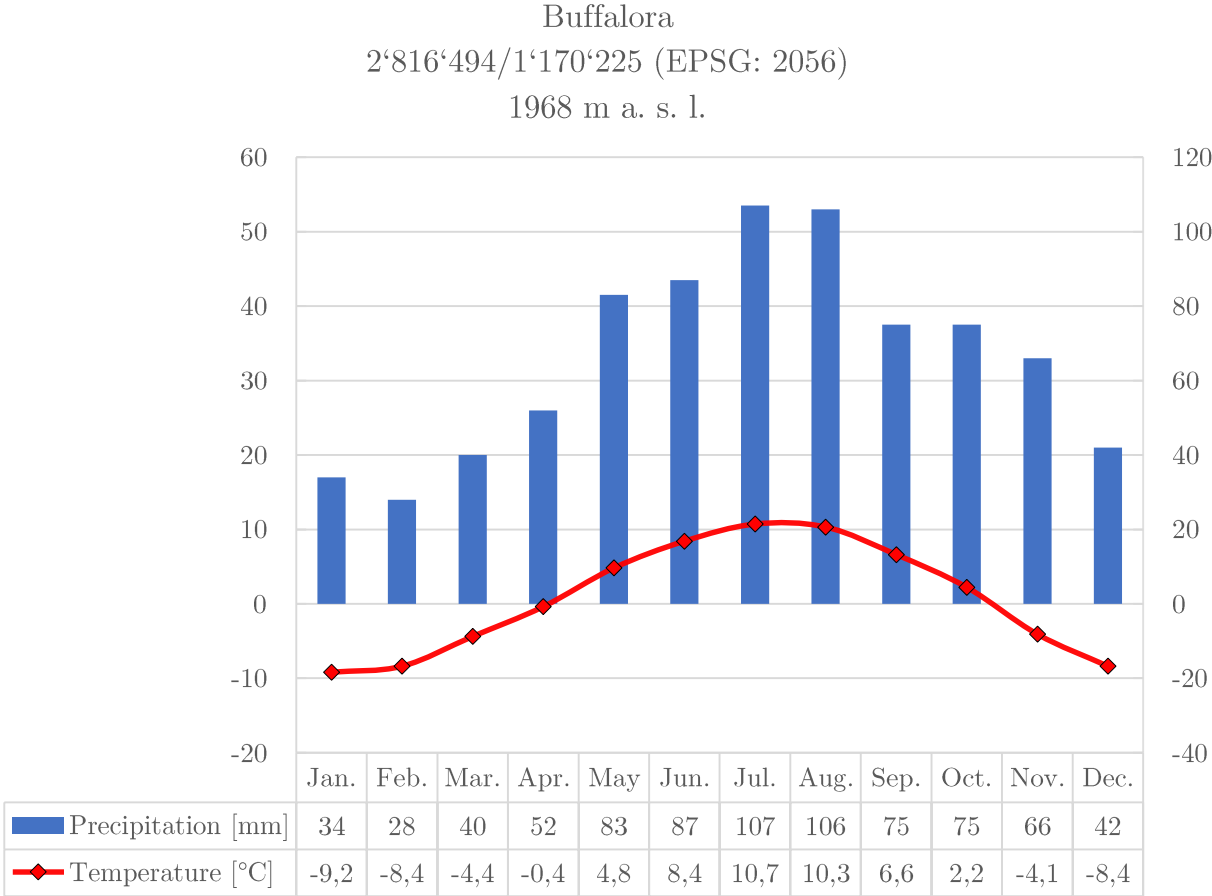


Figure 2: Climate chart Buffalora, long-term average 1980–2010 (own depiction based on MeteoSchweiz (2018b))

The research object within the research area is the approximately 7.5 ha big bed of the stream. The streambed was chosen because orthofotos revealed that due to the dense tree cover no bigger elevation changes had occurred beyond the stream bed in the last 20 years and because the terrain height is not detectable for the SfM-MVS method in densely vegetated areas (Fonstad et al., 2013).

Therefore, the models created and used in this work represent the actual, natural ground surface in the research object and are referred to as DTMs.

This clear delineation towards similar or sometimes synonymously used terms e.g. DEM is really important, since terms are not always employed identically across countries and especially the terms DEM and DTM are often erroneously used interchangeably (Li et al., 2005).

2.2 Data acquisition

This work uses three DTMs, of which two are LiDAR DTMs from the inventory of the SNP and one is the result of the SfM-MVS approach executed on the aerial photographs. The aerial photographs together with the GCPs were acquired during a 3.5 day field campaign. The first day in the beginning of June 2018 was used for an initial inspection of the stream, identifying the section that later was recorded and investigated. The actual data acquisition took place in the middle of August 2018. During 2.5 days all GCPs were placed, measured and removed as well as all aerial photos taken.

For the visual interpretation and the stream delineation SWISSIMAGE orthofotos for 2003 and 2009 and the SfM-MVS orthofoto for 2018 were used. The SfM-MVS orthofoto is one outcome of the modelling approach applied in this work and the SWISSIMAGE fotos are a part of the data provided by the SNP. For a detailed product information of SWISSIMAGE it is referred to Bundesamt für Landestopografie swisstopo (2010).

2.2.1 DTM from LiDAR

The two LiDAR DTMs are out of the inventory of the SNP and cover the year 2003 and 2009. The one from 2003 was commissioned by the swisstopo – the Federal Office of Topography – within the scope of swissALTI^{3D}. SwissALTI^{3D} is the nationwide high resolution DTM for Switzerland and for the year 2003 in our study area it has a resolution of 2 m with an accuracy of ± 0.5 m standard deviation (Bundesamt für Landestopografie swisstopo, 2012). The 2009 DTM was ordered by the SNP and has been created by BSF Swissphoto. It comes with a 1 m resolution and an accuracy of ± 0.06 m standard deviation (BSF Swissphoto AG/SPM/DET, 2009).

2.2.2 Aerial photos

Prior to the photo acquisition the segment was divided into seven subsegments. Thus, one subsegment could be covered within one drone flight, respectively with one battery. The planning of the subsegments and the flights including the flight path was done in the drone corresponding software AscTec Navigator, which was later also used to assign each picture its correct geolocation.

The drone used to capture the aerial photos was a Falcon 8 mounted with a Sony Alpha NEX-7 camera. Further specifications of the drone are displayed in table 1.

Table 1: Specifications Falcon 8 (adapted from Mancini et al. (2013) based on Ascending Technologies GmbH (2015))

Manufacturer	Ascending Technologies (Intel)
Type	V-Form Octocopter
Engine Power	8 Electric Brush-/Sensorless
Dimension and weight	770*820*125 mm, 2.3 kg (max. total take-off weight)
Fight mode	Dual (automatic based on waypoints or manual)
Endurance	12 – 20 min. ¹
Flexible camera configurations	Sony Alpha NEX-7 (focal length 27 mm), res. 6000*6000

¹ for SNP rather 6 – 12 min. because of the battery age and the elevation

The flight pass showed an 80 per cent overlap in flight direction, which is recommended by Kaiser et al. (2014), and good practise in the SNP, because it gives enough overlap for the SfM-MVS approach, and at the same time allows a decent coverage of the area within one flight (Westoby et al., 2012). Flight speed was set to 3.5 m/s to ensure enough time between each shot for the camera to process the pictures. This was especially important as the waypoints – points where the drone shots pictures – had to be placed dense to archive the 80 per cent overlap. Flight height was set to 50 m above ground (at the start position) resulting in a GSD of ~ 1.5 cm (cf. chapter Processing reports). According to Cawood et al. (2017) choosing a low flight height and a big overlap help to achieve a high precision in the later model. Flight segment three (part *Ova dal Fuorn* and *Ova da Val Ftur* confluence) was recorded twice as the last flight on the first flight day and as first flight of the second flight day, to ensure sufficient lighting conditions. A total of 735 photos was acquired.

2.2.3 Ground Control Points

To be able to georeference and validate the model, but also for the correction and validation of the camera alignment (cf. chapter 2.3.2 DTMs from aerial photos using SfM-MVS and chapter 2.4.2 Error metrics), a total of 66 GCPs in form of 10 by 10 cm big orange tiles (cf. figure 3) were placed and measured prior to the photo acquisition. The tiles were distributed evenly over the whole study object, approximately one each 40 m. Measuring was done using a GeoXR from Trimble with an external antenna (Zephyr 2). To achieve better results, the mean of at least 20 measurements over 20 – 35 seconds was taken (Fonstad et al., 2013). Except for two points all points could be measured with the Real Time Kinematic (RTK) fixed solution due to a satellite coverage of 6 – 13 satellites and network coverage. The points were labelled ascending in order of their acquisition. Point number



Figure 3: Exemplary GCP within the study object (photo taken by Daniel Thiex)

65b and 66 were measured without RTK fixed and later in a post processing corrected. In total a RMSE of 0.02 m for the horizontal accuracy as well as for the vertical accuracy could be reached.

Out of the 66 points four had to be discarded. These four points were rejected because they were not captured by any picture (nr. 34), were measured twice (nr. 9 and 10) or showed an inexplicable error in the processing of 10-fold higher than all other points (nr. 1). The problems with point number one might be explained by a not fully ready Global Positioning System (GPS) device, as it was the first point measured during the campaign. To not falsify the results and because the remaining amount of points was still sufficient, point number one was ignored. The discarded points 9 and 10 were averaged to a new point 9a. With this new point and minus the four discarded ones a total of 63 points remained for the georeferencing and the validation.

Of the 63 points 21 were randomly selected and kept back for the validation of the model. To keep 33.3 per cent of points back for the validation is in the magnitude of other works that used 37 per cent (Mali and Kuiry, 2018) or 30 to 35 per cent (Javernick et al., 2016). The remaining 42 points were grouped into four scenarios A, B, C and D (cf. figures 4–7). Each of the scenarios is having a different amount (42, 21, 21, 11) of GCPs and a varying distribution (two times uniform (following referred to as uniform), two times in the top, middle and bottom part of the study object (following referred to as tmb)). The chosen distributions were expert based on the basis of James and Robson (2012), who state that a dispersed distribution with some at the borders of the object minimizes the georeferencing error. Scenarios B, C, D were all subsamples of A: B being a random selection of A; C and D a manual of A, so that each had three, respectively six points located in the top and bottom parts, and five, respectively 10 in the middle part of the study object (cf.

figures 5 – 7).

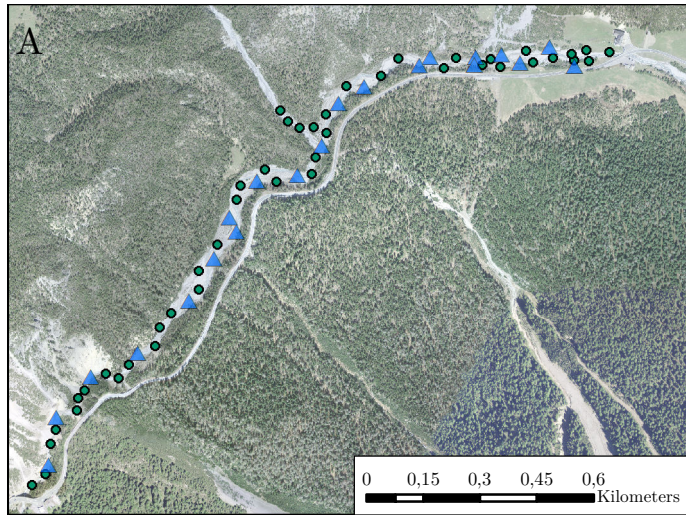


Figure 4: GCPs of the all scenario (A), 42 reference points (green dots) and 21 validation points (blue triangles)(own depiction, data basis: GPS measurements, SNP SWISSIMAGE 2015)

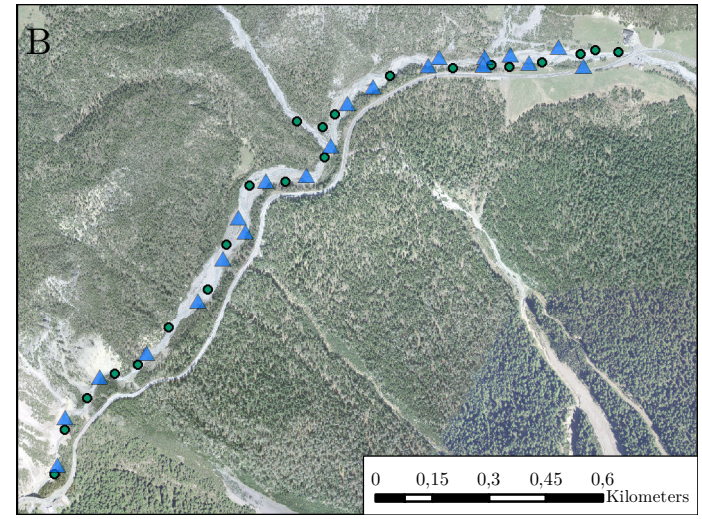


Figure 5: GCPs of the half uniform scenario (B), 21 reference points (green dots) and 21 validation points (blue triangles)(own depiction, data basis: GPS measurements, SNP SWISSIMAGE 2015)

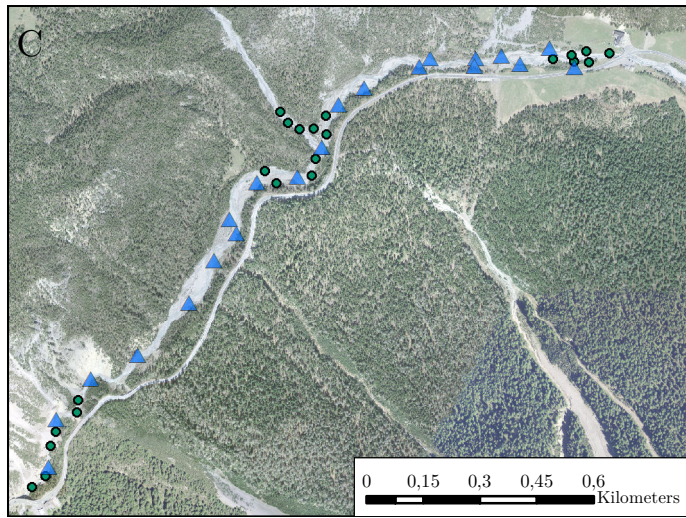


Figure 6: GCPs of the half tmb scenario (C), 21 reference points (green dots) and 21 validation points (blue triangles)(own depiction, data basis: GPS measurements, SNP SWISSIMAGE 2015)

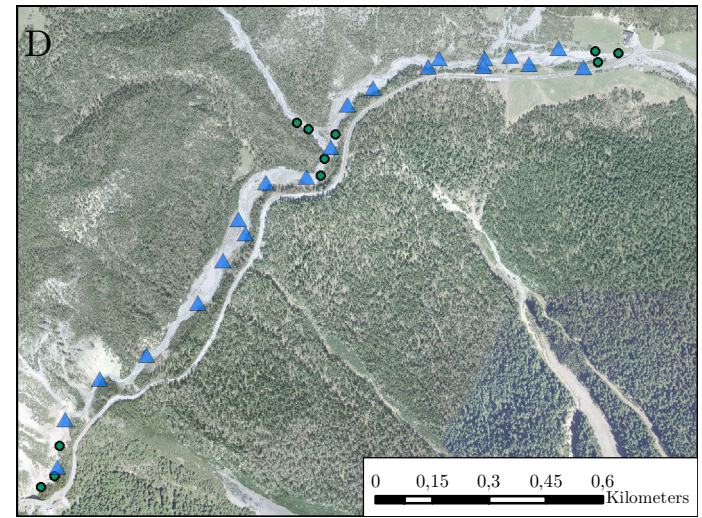


Figure 7: GCPs of the quarter tmb scenario (D), 21 reference points (green dots) and 21 validation points (blue triangles)(own depiction, data basis: GPS measurements, SNP SWISSIMAGE 2015)

2.3 Processing

2.3.1 Pix4Dmapper and PhotoScan

There is a good deal of free and commercial software available to process aerial photographs. Even though freeware comes with no costs and the algorithms used in the single steps are more comprehensible only few works solely rely on those (cf. James and Robson, 2012; Stumpf et al., 2015; Micheletti et al., 2015). This surprises because according to Jaud et al. (2016) as well as Mali and Kuiry (2018), who tested freeware against commercial software, both – free and commercial – show equally good results in means of accuracy. Still both studies acknowledge commercial software has a better handling of the dome effect – the effect of having positive errors in the centre of the model decreasing towards the sides where there are negative errors. Others on the other hand expect the precision to be better in commercial software (James and Robson, 2012; Martínez-Carricondo et al., 2018) and praise especially PhotoScan to have a user friendly graphical interface (Javernick et al., 2014) and higher alignment capabilities – compared to freeware (Kaiser et al., 2014). This discrepancy might find its explanation in the facts that each study uses a different study area with varying geomorphological features, not the same specific software settings and that there is so much software available that almost never exactly the same software packages are compared.

In this work, two commercially available software packages were used to process the aerial photographs namely Agisoft PhotoScan (Version 1.2.6 build 2834 released on the 20.07.2016), in this work reduced to PhotoScan, and Pix4Dmapper (Version 4.3.31 released on the 16.10.2018). In tables sometimes Pix4Dmapper is referred to as Pix4D and PhotoScan as AgiSoft.

The decision to compare those two programmes was based on the facts that these are the ones mainly applied in science (Pix4Dmapper (Chesley et al., 2017; Eltner et al., 2014; Ruzgienė et al., 2015); PhotoScan (Cook, 2017; Javernick et al., 2016; Martínez-Carricondo et al., 2018)), that especially PhotoScan is widely used in the field of Geomorphology (Cook, 2017), and that to the authors best knowledge both have not been compared on their performance in an mountain stream environment yet. A further point not to be neglected is that these are the two programmes available at the supervising institutions – with different experience about the performance – and because of that they could be tested free of the usually incurring costs. The institute of geography in Tübingen uses PhotoScan and the SNP uses Pix4Dmapper.

2.3.2 DTMs from aerial photos using SfM-MVS

The method SfM-MVS used and later described in this work is allocated in the field of photogrammetry and has its origins in the late 1970s (Ullman, 1979; Westoby et al., 2012). Strictly speaking it consists of two parts: Structure from Motion (SfM) and Multi-View Stereo (MVS). SfM was first discussed by Ullman (1979) and deals with a computational recognition of image elements over time, respectively movement, hence the name SfM (Ullman, 1979). Once the image elements are recognized the MVS takes place where noise is filtered and the number of identified image elements is increased (James and Robson, 2012). A good comparison of early MVS algorithms is given by Seitz et al. (2006). Despite having the MVS approach implemented, some studies only use the term SfM (cf. Eltner et al., 2014; Martínez-Carricondo et al., 2018). In this work solely SfM-MVS is used to emphasize that MVS is a main part of the workflow and to stress that not only the SfM part was carried out.

Although the workflow varies slightly between software packages (Carrivick et al., 2016), it can be summarized into five necessary steps following Chesley et al. (2017):

- 1) identification of keypoints in single images;
- 2) matching of identical keypoints amongst images;
- 3) estimation of the camera position;
- 4) creation of a point cloud from the oriented images (MVS part);
- 5) creation and export of the model (DTM, orthomosaic).

These 5 steps are partly an own independent processing task in Pix4Dmapper and PhotoScan and partly more of them are implemented in one task.

Figure 8 displays the detailed workflow this work followed for both programmes. Of the five necessary steps one to three are a part of the first task (*Align Photos*). Step 4 can be found in the *Build Dense Point Cloud* task and step five in the last task *Build DTM*. All other tasks executed serve the georeferencing of the model (e.g. *Place Markers*) or the quality improvement of the model (e.g. *Classifying Dense Cloud Points*). The major difference in the executed workflow is that with *Build Mesh* and *Classifying Dense Cloud Points* PhotoScan has two more individual tasks. In Pix4Dmapper both of these points are executed as a part of the step 2. *Point Cloud and Mesh* (cf. figure 8).

Because a good and detailed description of the single steps is given by James and Robson (2012) or Westoby et al. (2012) and both user manuals (Agisoft, 2018; Pix4D, 2017) are here very detailed, only settings are mentioned where the default values were changed. As the detailed settings used in the single steps are rarely included in any paper and it is therefore, impossible to build upon others experiences, the recommendation of the

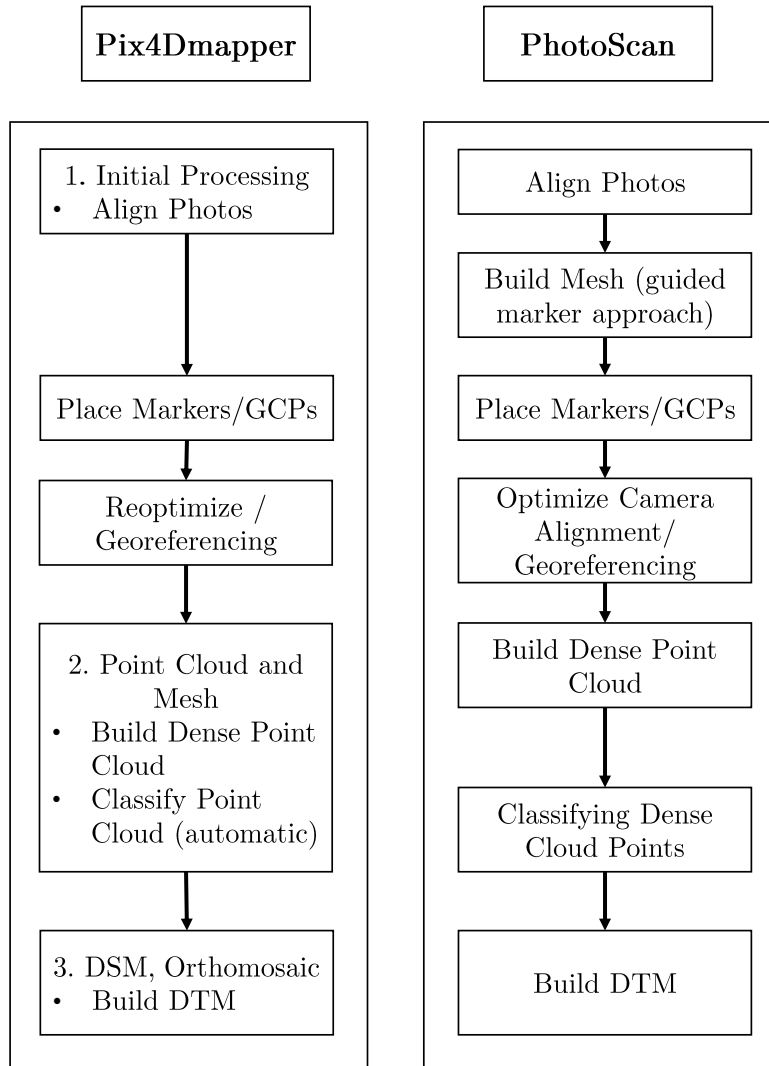


Figure 8: Workflow with all processing tasks executed in Pix4Dmapper and PhotoScan (own depiction based on Agisoft (2018) and Pix4D (2017))

manuals were followed unless mentioned otherwise. For PhotoScan this means in the task *Build Dense Point Cloud* the depth filtering was set to mild to make sure small details were not to be sorted out (Agisoft, 2018). For Pix4Dmapper this means in step two to enable the point cloud classification, and in step three to disable the contour lines for the DTM as they were of no interest for the comparison of the DTMs (cf. chapter 3.3 Change analysis 2003–2018). The settings for the point cloud densification image scale and the point cloud classification are described in the results as finding the correct ones was part of this work.

To save processing time while testing the default settings the whole workflow was first carried out with a small subset of photos. In total – excluding one of the two times acquired

flight segment 3–636 pictures were used for processing. For segment three the pictures from the first day were chosen. Compared to the second day the pictures contain fewer shadows, which minimizes the problem of a moving shadow (Mali and Kuiry, 2018) and produces better results (Agisoft, 2018).

The calculations for both programmes was performed on the supercomputer of the geography institute in Tübingen, which is equipped with an Intel® Core™i7-980 (3.33 GHz, 6cores/12threads) processor, 48 GB of RAM, a 64-bit operation system (Windows 10) and a 3GB NVIDIA GeForce GTX 580 graphic card. To save processing time the images and the results of all calculations were saved on a SSD (Samsung 850 EVO) hard drive as recommended by the Pix4D support (Pix4D, 2019b).

Because of the long processing time of over 17 hours in PhotoScan for the dense point cloud these were only calculated for the best GCP setting (cf. chapter 3.1.3 Model quality). All explicit settings for the two runs—one in Pix4Dmapper and one in PhotoScan—can be found in the two processing reports in the appendix (cf. chapter Processing reports).

2.3.3 DTMs of Difference

To be able to evaluate the elevation changes over the years the two LiDAR DTMs and the SfM-MVS DTMs were compared. Following the temporal development the 2003 DTM was compared with the 2009 one and the 2009 DTM with the 2018 one. The comparison was done via DoDs. DoDs are the result of two DTMs being subtracted from each other. To be able to subtract the DTMs they need to have the same resolution and processing extend. Therefore, the 2018 DTM was downsampled to a 1 m resolution and the 2009 to a 2 m resolution. The downsampling was done in the latest version of SAGA (7.2.0) (Conrad et al., 2015)—a free open source Geographic Information System (GIS) software—using bilinear interpolation. Bilinear interpolation was chosen because it best preserves accuracy and terrain characteristics (USGS, n.y.). For the 2018 DTM in the change detection the one created with Pix4D and the GCP all scenario was chosen, as it showed to have the best model quality (cf. chapter 3.1.3 Model quality)

Before the calculation of each DoD the stream was masked and in all DTMs removed, leaving for 2003–2009 an area of 5.52 ha and for 2009–2018 an area of 5.56 ha. This was done because in both—LiDAR and SfM-MVS—DTMs running water represents a problem (Bundesamt für Landestopografie swisstopo, 2018; Cook, 2017). On the one hand this can be explained with the nature of the water absorbing and scattering the incoming light leading to a lower point density (Fonstad et al., 2013) and on the other hand because for

matching points in overlapping pictures there is a high colour, brightness and elevation variation due to the movement of the water (Javernick et al., 2016). The stream boundaries were digitalized using SWISSIMAGE orthofotos (2003 and 2009) and the SfM-MVS orthofoto (2018) on a digitizing scale of 1:400. The digitizing, masking and the DoD calculation using the Raster Calculator tool – a tool that allows to execute mathematical operations on raster cells – were performed using ArcMap 10.3.1 from ESRI (Environmental Systems Research Institute, 2015).

To be able to quantify the changes in the DoDs the volume of the change in cubic metre was calculated. Therefore, the study object was first divided into five approximate equal sections (I–V). The middle section covers the *Ova da Val Ftur/Ova dal Fuorn* confluence and a small part before and afterwards. The segments above and below were divided in a way that the upper division was placed in the narrowest part and for the lower division the boundary was set at the part where the river becomes narrower again. Afterwards all positive, respectively negative values above the DT were added for each DoD (cf. chapter 2.4.3 DoDs detection threshold).

2.4 Validation

2.4.1 Software comparison

Comparing two software programmes holistically can be a challenge when it comes to subjective parts such as user friendliness or the quality of the graphical user interface as these differ between users. To be able to evaluate those parts as objectively as possible a table including evidence for all positive and negative points found while using each software was created and used for the validation.

Still the selection of the points remains subjective though expert based, and therefore, a bigger weight was given to the results of the performance comparison. Here the calculation time for the single steps and the model quality of the four GCP scenarios were examined.

Because the price of the software also influences the decision which one to buy and finally use, the price of the software for the different available package options was added to the comparison.

2.4.2 Error metrics

In modelling it is important to implement a validation of the model, respectively test its accuracy (Mali and Kuiry, 2018). Consequently, one can not only be sure there was no mistake done during the modelling – this is especially important since some main parts of the SfM-MVS approach are still a black box (Smith et al., 2016) – but it also allows to make statements about the achieved quality of the model. The validation can be implemented on various stages of the workflow. Mancini et al. (2013) for example evaluate the point cloud. For this work it was decided to evaluate the final outcome of the SfM-MVS method, the DTM. This decision was based on the two LiDAR DTMs only being available as raster and following Kaiser et al. (2014), who consider rasters a good terrain description and thus being sufficient for an accuracy assessment. As the DTM produced is used for further analysis this knowledge allows us to put the results into perspective.

As error metric most works that address the DTM quality solely rely on the RMSE (Agüera-Vega et al., 2017; Martínez-Carricondo et al., 2018; Uysal et al., 2015). Following Chai and Draxler (2014) the RMSE has its advantages for example not using absolute values or being good at revealing model performance differences and as it is as output already implemented in Pix4Dmapper, easy to use. Still using one metric only emphasizes a certain aspect of the error characteristics and a combination of metrics is always recommended (Chai and Draxler, 2014). Hence, for the evaluation of the model performance of the four settings in Pix4Dmapper and PhotoScan two metrics were considered: the MAE recommended by Willmott and Matsuura (2005) and the above mentioned RMSE. The universal version of both equations is displayed in (a) and (b).

$$\text{RMSE} = \sqrt{\frac{\sum_{i=1}^n (P_i - O_i)^2}{n}} \quad (\text{a})$$

$$\text{MAE} = \frac{\sum_{i=1}^n |P_i - O_i|}{n} \quad (\text{b})$$

with

n: number of samples

P_i : model predictions of the i^{th} sample

O_i : in field measured value for the i^{th} sample

Adapted to the 21 GCPs (n=21) – those that were kept back for the validation – the X, Y, and Z coordinates are each deployed for P_i , respectively O_i to calculate the error of

the model in X direction ($RMSE_x$, MAE_x), Y direction ($RMSE_y$, MAE_y) and Z direction ($RMSE_z$, MAE_z).

To get the overall error for all three dimensions of the GCPs, the Euclidean distance with dimension three was applied for the difference between the predicted coordinate and the coordinate measured with a GPS (Hieber, 2018). For the RMSE the resulting equation (c) is described in Martínez-Carricondo et al. (2018) and for the MAE (d) it was adopted accordingly .

$$RMSE_{xyz} = \sqrt{\frac{\sum_{i=1}^n [(X_{Mi} - X_{GPSi})^2 + (Y_{Mi} - Y_{GPSi})^2 + (Z_{Mi} - Z_{GPSi})^2]}{n}} \quad (c)$$

$$MAE_{xyz} = \frac{\sum_{i=1}^n |\sqrt{[(X_{Mi} - X_{GPSi})^2 + (Y_{Mi} - Y_{GPSi})^2 + (Z_{Mi} - Z_{GPSi})^2]}|}{n} \quad (d)$$

with

X_{Mi}, Y_{Mi}, Z_{Mi} : X, Y and Z coordinates of the i^{th} GCP in the model prediction

$X_{GPSi}, Y_{GPSi}, Z_{GPSi}$: X, Y and Z coordinates measured with GPS for the i^{th} GCP

To access the quality of the georeferencing algorithms of both programmes – how well the software manages to link the model to the real world – the same metrics were further used on the 41, respectively 21 (2x)/11 georeferencing points after referencing. All statistical analysis was done using the programming language R (R Core Team, 2018).

2.4.3 DoDs detection threshold

As all input DTMs come with an error and as a DoD is a combination of two DTMs, it is likely that an DoD contains an error as well. It is important to know the magnitude of the error to be able to differentiate between actual surface changes and artefacts caused by the error. In this work the minimum level of detection was applied, a simple but widely used and accepted method (Williams, 2012). For the minimum level of detection the combined error for each DoD is calculated using the following equation (e) by Williams (2012)

$$\delta U_{DoD} = \sqrt{\delta z_1^2 + \delta z_2^2} \quad (e)$$

with

δz_1 : error of the first DTM

δz_2 : error of the second DTM

δU_{DoD} : combined error of the DoD

Deploying equation (e) to the DTMs results in δU_{DoDs} of:

- ± 0.50 m for 2009-2003
- ± 0.08 m for 2018-2009
- ± 0.07 m for the Pix4Dmapper DTM-PhotoScan DTM

These values are taken as a threshold where changes beyond can be reliably accepted.

3 Results

3.1 Pix4Dmapper versus PhotoScan

3.1.1 Software properties and settings

As displayed in table 2 both Pix4D and Agisoft provide their users with a manual. Offering 305 pages Pix4D’s manual is two times more extensive than Agisoft (127 pages). The

Table 2: Comparison of noticeable software properties (own findings while executing the workflow in each programme)

	Pix4Dmapper	PhotoScan
Documentation	305-page manual including a lot of online references ¹	127-page manual with few online references ²
Handling and clarity	straightforward navigation in model, responsive while processing, detailed processing graph	complex navigation in model, blocked while processing, simple processing graph
Workflow	can run fully automated	step by step execution
GCP weighting	GCPs identified on a greater zoom level are given a higher weight ³	weights all GCPs the same
GCP error export	table included in the processing report	export as separate table
Point cloud densification	failed on original image size	successfully processed original image size
Point cloud classification	automatic	manual
DTM resolution	minimum 5*GSD ¹	GSD ²

¹ Pix4D (2017)

² Agisoft (2018)

³ Pix4D (2019a)

navigation of the model in Pix4Dmapper is intuitive and straightforward as the options

zoom, pan and turn are all accessible with the mouse without further changes. Beside that, the programme is responsive while processing. For a good orientation of the current processing step a detailed processing graph is given. In PhotoScan the navigation of the model is more complicated compared to Pix4Dmapper because the navigation options is divided into submenus. Additionally, the programme can not be used while calculations are being executed. The processing graph in form of a single progress bar and the description of the current calculation step are kept simple. In both programmes the single tasks of the workflow can be executed step by step and in addition Pix4Dmapper has a fully automated option implemented. The automation is also included in Pix4Dmapper when it comes to the classification of the point cloud. The result of the classification in Pix4Dmapper for this work was unsatisfying, especially with regard to the area of the alluvial fan points of the scarps falsely being classified as human objects (turquoise) or at the sides of the streambank points being erroneously assigned to the group building (purple) (cf. figure 9). Because in Pix4Dmapper only points from the ground and road

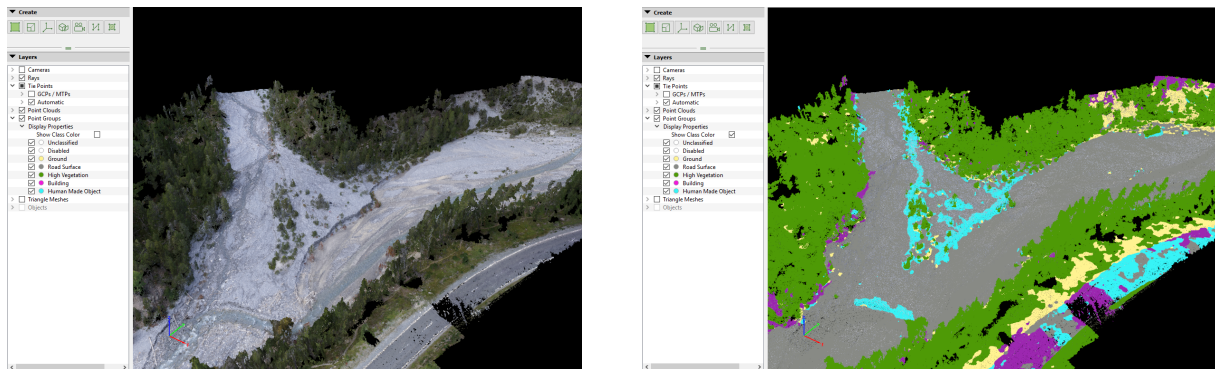


Figure 9: Point Cloud Classification in Pix4Dmapper: true colour model (left), classified point cloud (right) (screenshot graphical user interface Pix4Dmapper)

surface type are preserved in the DTM (Pix4D, 2019b), the classified point cloud had to be post corrected. Therefore, all points that were classified as human object or building where assigned to the class ground. This simple workaround was possible since there were no anthropogenic features present in the the study object. In PhotoScan the classification has to be done manually by setting three parameters (maximum angle, maximum distance and cell size) (cf. table 2). The finding of the best value combination is an elaborate process and the settings differ for each study object. For the *Ova dal Furon 15* the maximum angle, 0.5 for the maximum distance and six for the cell size proved to deliver the best results. Here the scarps and stones were still classified as ground points but deadwood and trees in the stream bed as object to be removed (cf. figure 10). Higher numbers in the cell size led to a classification of all points, whereas smaller numbers in the maximum distance to a wrong classification of the scarps and trees in the stream bed. Increasing

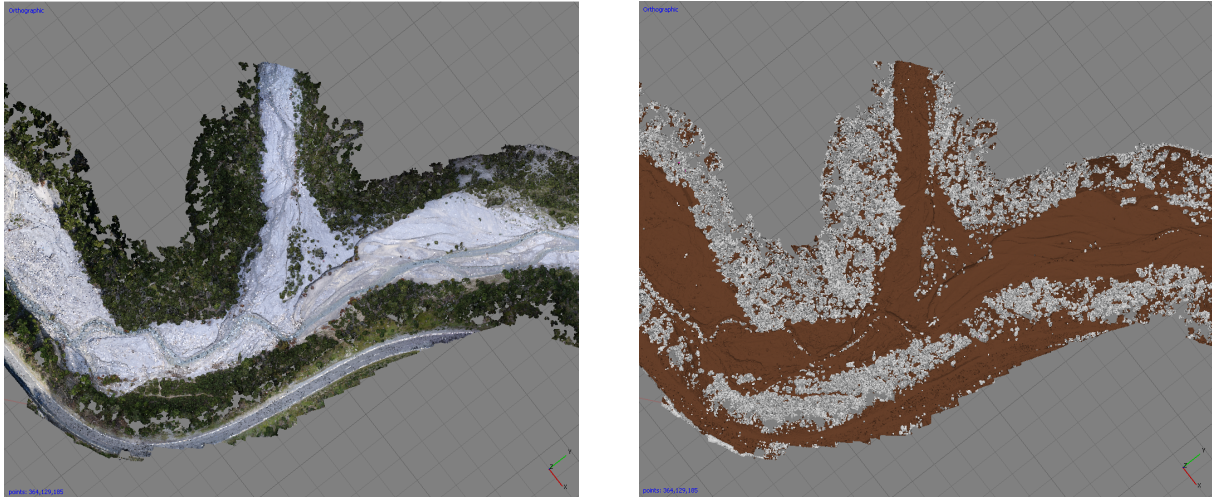


Figure 10: Point Cloud Classification in PhotoScan: true colour model (left), classified ground points (brown) (right) (screenshot graphical user interface PhotoScan)

the maximum angle did not show any improvement. In PhotoScan all GCPs chosen for georeferencing are weighted the same and an export into a separate table is possible. In Pix4Dmapper pictures where the GCPs were identified on a higher zoom level are taken into account to a larger degree. A separate export in a table is not possible and the error is solely printed in the processing report. In PhotoScan the DTM can be exported in the resolution of the GSD, in Pix4Dmapper the GSD has to be set to a minimum of five times (cf. table 2).

For the image scale in the point cloud densification step the settings in Pix4Dmapper were set to the default half image size because with the original image size led to a programme failure. In PhotoScan the original image size could be successfully processed.

3.1.2 Processing time

In total a processing time of around 7 hours in Pix4Dmapper is to be compared by a processing time of around 21 hours in PhotoScan. In Pix4Dmapper the point cloud densification and the DTM processing take most of the time with around 2.5 hours each. The orthomosaic generation accounts for about another 2 hours and the point cloud classification took another 15 minutes. For PhotoScan the biggest part of the 21 hours are needed for the dense point cloud calculation (~ 17 hours), a smaller part for the matching and alignment (~ 2 hours) and the DTM processing (~ 1 hour). The orthomosaic (less than 30 minutes) and the optimization time (17 seconds) contribute an almost negligible part (cf.

table 3). Despite their mathematical incontestability these numbers have to be treated with caution and a direct comparison of them is not advisable (cf. 4.1.2 Processing time).

Table 3: Processing times (hh:mm:ss) for both programmes (own depiction, data basis: processing reports cf. Appendix)

	Pix4Dmapper	PhotoScan
matching and alignment	—	01:46:02
optimization time	—	00:00:17
dense point cloud (depth maps, dense cloud)	—	17:48:00
point cloud densification	02:43:03	—
point cloud classification	00:15:03	—
DTM processing	02:26:29	00:57:04
Orthomosaic generation	01:49:21	00:25:07
Total	07:13:56	20:56:30

3.1.3 Model quality

In total, for both programmes the RMSE of the georeferencing GCPs as well as the MAE of the georeferencing GCPs is ranging from 0.01 m to 0.10 m. For all four settings PhotoScan has an equal or slightly higher error of a few centimetres compared to Pix4Dmapper. The best referenced model, respectively the smallest error was for both programmes reached for the setting with 11 GCPs (quarter tmb) and lays in the magnitude of between 0.01 m and 0.04 m. The highest error in Pix4Dmapper is with 0.05 m in the all scenario, for PhotoScan in the half tmb scenario with 0.10 m (cf. tables 4 and 5).

Table 4: RMSE [m] of the georeferencing GCPs (own calculations)

	Pix4D	AgiSoft	Pix4D	AgiSoft	Pix4D	AgiSoft	Pix4D	AgiSoft
Setting	all		half uniform		half tmb		quarter tmb	
[GCPs]	[42]		[21]		[21]		[11]	
RMSE _{xyz}	0.05	0.05	0.04	0.06	0.04	0.10	0.02	0.04
RMSE _x	0.02	0.02	0.02	0.02	0.01	0.03	0.01	0.02
RMSE _y	0.04	0.04	0.03	0.05	0.02	0.04	0.01	0.02
RMSE _z	0.02	0.03	0.02	0.03	0.03	0.08	0.01	0.04

The RMSE and the MAE ranges from 0.01 m up to 0.79 m for the validation points. As already noticed with the georeferencing PhotoScan has also higher errors here compared to Pix4Dmapper. An exception is the half tmb scenario. Here the RMSE as well as the MAE are slightly lower than the Pix4Dmapper values. The lowest errors are reached for

Table 5: MAE [m] of the georeferencing GCPs (own calculations)

	Pix4D	AgiSoft	Pix4D	AgiSoft	Pix4D	AgiSoft	Pix4D	AgiSoft
Setting	all		half uniform		half tmb		quarter tmb	
[GCPs]	[42]		[21]		[21]		[11]	
MAE _{xyz}	0.03	0.04	0.03	0.04	0.03	0.07	0.02	0.04
MAE _x	0.01	0.02	0.01	0.02	0.01	0.02	0.01	0.01
MAE _y	0.02	0.02	0.02	0.03	0.02	0.03	0.01	0.01
MAE _z	0.02	0.02	0.02	0.02	0.02	0.06	0.01	0.02

both programmes for the all setting with 42 georeference points, the highest for the quarter tmb setting with values up to 0.79 m. Comparing the half uniform and half tmb settings, PhotoScan performs slightly better on the half tmb whereas Pix4Dmapper is better in the half uniform setting. Except in the setting half tmb where the RMSE_x accounts for the biggest part of the overall error, for all other settings the error in Z direction has the biggest impact in both programmes (cf. tables 6 and 7).

Table 6: RMSE [m] for the 21 validation points (own calculations)

	Pix4D	AgiSoft	Pix4D	AgiSoft	Pix4D	AgiSoft	Pix4D	AgiSoft
Setting	all		half uniform		half tmb		quarter tmb	
[GCPs]	[42]		[21]		[21]		[11]	
RMSE _{xyz}	0.05	0.05	0.13	0.16	0.16	0.13	0.50	0.79
RMSE _x	0.02	0.02	0.03	0.03	0.12	0.08	0.25	0.08
RMSE _y	0.02	0.03	0.06	0.06	0.07	0.06	0.13	0.18
RMSE _z	0.04	0.04	0.11	0.14	0.08	0.09	0.41	0.76

Table 7: MAE [m] for the 21 validation points (own calculations)

	Pix4D	AgiSoft	Pix4D	AgiSoft	Pix4D	AgiSoft	Pix4D	AgiSoft
Setting	all		half uniform		half tmb		quarter tmb	
[GCPs]	[42]		[21]		[21]		[11]	
MAE _{xyz}	0.04	0.05	0.10	0.12	0.14	0.11	0.36	0.52
MAE _x	0.01	0.02	0.02	0.02	0.09	0.05	0.19	0.06
MAE _y	0.01	0.02	0.04	0.04	0.05	0.04	0.08	0.12
MAE _z	0.03	0.03	0.09	0.10	0.07	0.07	0.27	0.49

Comparing the RMSE_{xyz} and the MAE_{xyz} between georeferencing and validation, table 8 shows that for all the settings both error metrics are in a similar range. For the georeferencing this is between 0.03 m and 0.05 and for the validation it is between 0.04 m and 0.05 m. Whereas for the georeferencing the error only slightly changes with decreasing

number of GCPs, for the validation points a rise can be observed (cf. table 8).

Table 8: $RMSE_{xyz}$ [m] and MAE_{xyz} [m] for the georeferencing points and for the validation points (own calculations)

	Pix4D	AgiSoft	Pix4D	AgiSoft	Pix4D	AgiSoft	Pix4D	AgiSoft
Setting	all		half uniform		half tmb		quarter tmb	
[GCPs]	[42]		[21]		[21]		[11]	
$RMSE_{xyz}^1$	0.05	0.05	0.04	0.06	0.04	0.10	0.02	0.04
MAE_{xyz}^1	0.03	0.04	0.03	0.04	0.03	0.07	0.02	0.04
$RMSE_{xyz}^2$	0.05	0.05	0.13	0.16	0.16	0.13	0.50	0.79
MAE_{xyz}^2	0.04	0.05	0.10	0.12	0.14	0.11	0.36	0.52

¹ Georeferencing

² Validation

3.1.4 Software pricing

As displayed in table 9 PhotoScan and Pix4Dmapper sell different packages and subscription options. Both offer full functioning trials: Pix4Dmapper for 15 days, PhotoScan for 30 days. Comparing the price the professional edition for PhotoScan is in the standard version cheaper by 877 € than for Pix4Dmapper. PhotoScan offers an educational version for usage in science, Pix4Dmapper offers a suitable solution for the usage of the software in teaching. Where PhotoScan offers a basic version, Pix4Dmapper has the possibility of a monthly subscription.

The recommended system requirements are for both programmes high. It is advised to have a CPU with several cores and both programmes are able to draw back on the GPU for additional processing power. For a smooth processing of 500 pictures 32 GB of RAM are needed (cf. table 9).

Table 9: Pricing and system requirements for Pix4Dmapper and PhotoScan (own depiction based on Agisoft LLC (2019) and Pix4D SA (2019))

	Pix4Dmapper	PhotoScan¹
Pricing		
Trial	15 days (full function)	30 days (full function)
Standard Edition (very basic tools, lifetime licence)	—	159 €, 52 € (educational)
Professional Edition (lifetime licence)	3 990 €, 1 500 € (2 devices, professor licence), 5 000 € (25 devices, classroom)	3 113 €, 488 € (educational)
Subscription (per month)	260 € (2 devices)	—
System requirements		
CPU	quad-core or hexa-core (Intel i7/i9 or similar)	multi core (3GHz+)
able to use the GPU	Yes (needs to be compatible with OpenGL)	Yes (needs to be compatible with OpenGL)
RAM	32 GB (500–2 000 pictures)	32 GB (500 pictures)

¹ The price for PhotoScan fluctuates due to the dollar/euro conversion rate.

3.2 DTMs from aerial photos using SfM-MVS

Finally both programmes successfully produced a high resolution DTM with a 7.6 cm pixel resolution (5*GSD) in Pix4Dmapper and 1.49 cm pixel resolution (GSD) in PhotoScan (cf. processing reports in the appendix). For both programmes the DTM for the GCP all scenario is displayed here because it is the one with the lowest error rate (cf. 3.1.3 Model quality) and the one later used in the change detection analysis. For a better visual interpretation the shaded relief was underlaid and for PhotoScan the DTM was exported with a two time GSD resolution to save processing time and to provide an easier handling in the GIS (cf. figures 11 and 12).

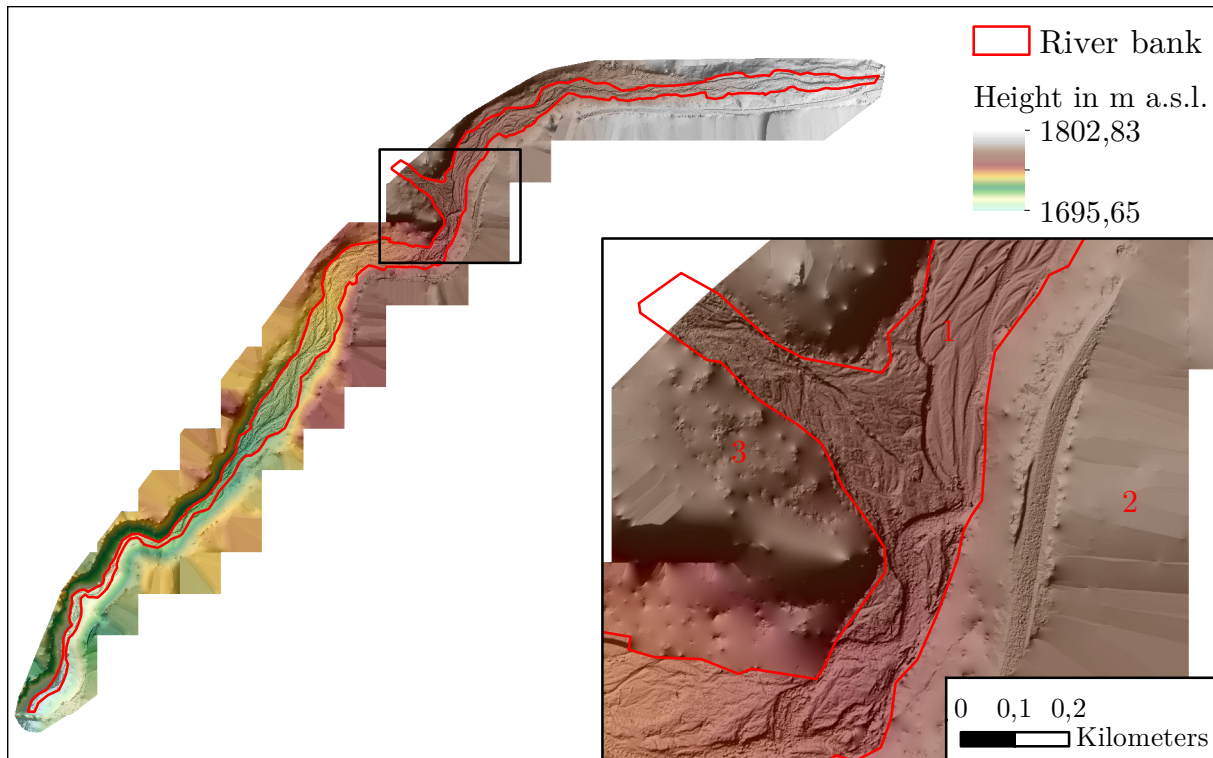


Figure 11: DTM from SfM-MVS created with Pix4Dmapper, 7.6 cm pixel resolution, all scenario (own depiction, data basis: Pix4Dmapper DTM, river bank delineation 2018)

Figure 11 shows the DTM created in Pix4Dmapper for the all scenario. The enlargement displays that the created DTM can be roughly separated into three parts:

- A well represented part where waterlines are recognizable in the area of the stream bank (1),
- an artefactic one where Pix4Dmapper added area that was not successfully covered by the SfM-MVS approach (2),
- and one closely above the stream bank where the vegetation was filtered and the ground surface is displayed but with tree remains as artefacts (3).

Applying the same delineation to the DTM created with PhotoScan (cf. figure 12) one can recognize a coarser surface in all areas with the waterlines still discernible (1). Contrary to Pix4Dmapper, PhotoScan in general has a narrower delineation of the reconstructed area (2 and 4) but has a less strict delineation at the edges of the study area where only few pictures were available (5). In the range above the stream bank (3) the surface is coarser than in Pix4Dmapper and there are several patches of areas that could not be properly reconstructed.

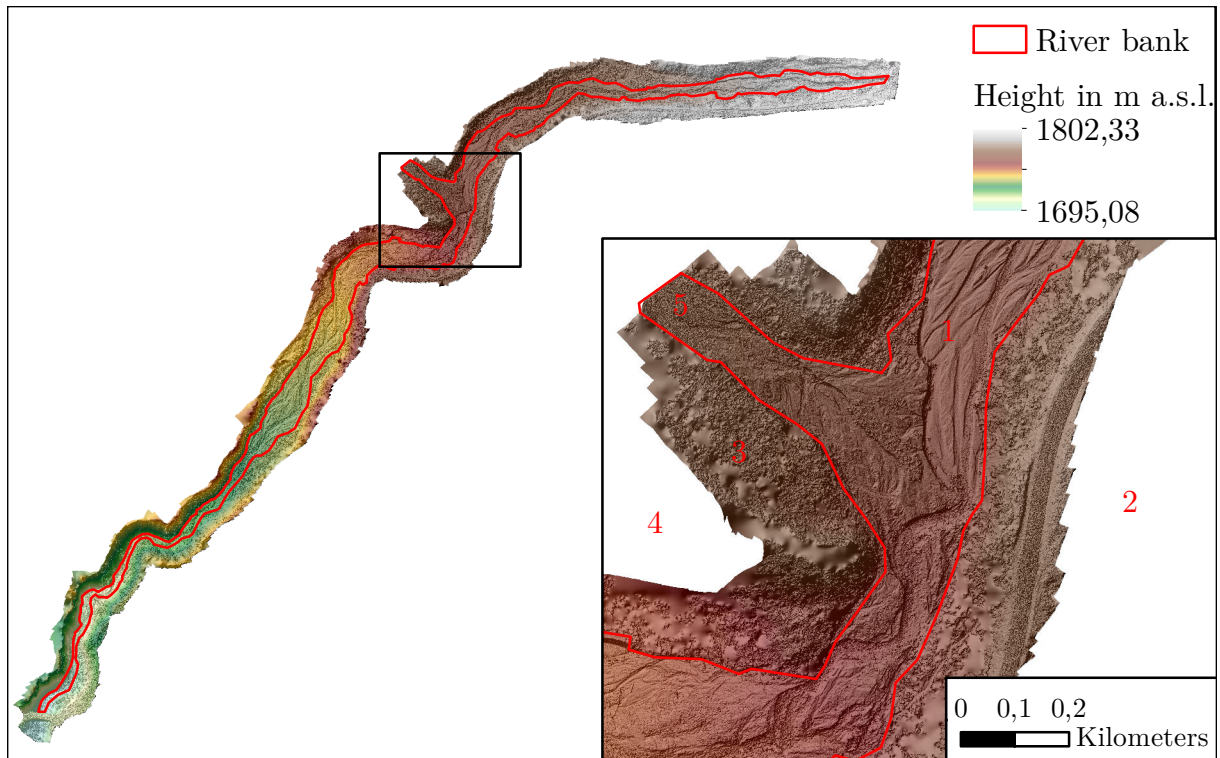


Figure 12: DTM from SfM-MVS created with PhotoScan, 2.97 cm pixel resolution, all scenario (own depiction, data basis: PhotoScan DTM, river bank delineation 2018)

Comparing both DTMs via a DoD Figure 13 shows that the most differences occur in sections II–IV and are up to 1.32 m. Taking a closer look at the differences above the DT of ± 0.064 m in the enlargements 1 and 2 shows that the changes outside the stream area are positive. Here PhotoScan calculated higher elevations compared to Pix4Dmapper. Inside the stream there are mainly negative values, which correspond to higher values in Pix4Dmapper compared to PhotoScan. In total the differences range from -2.38 m up to 3.82 m. Matching the differences of the DoD with the corresponding orthofoto the consistent patches outside the stream can be linked to bushes in the stream bed (cf. enlargements 1 and 2) (cf. figure 13).

The histogram of the DoD PhotoScan-Pix4Dmapper shows that the most differences between the two DTMs are below the DT, respectively between -0.064 m and 0.064 m. Above the DT there are more positive than negative values. There are almost no values below -0.25 m and above 0.5 m (cf. figure 14).

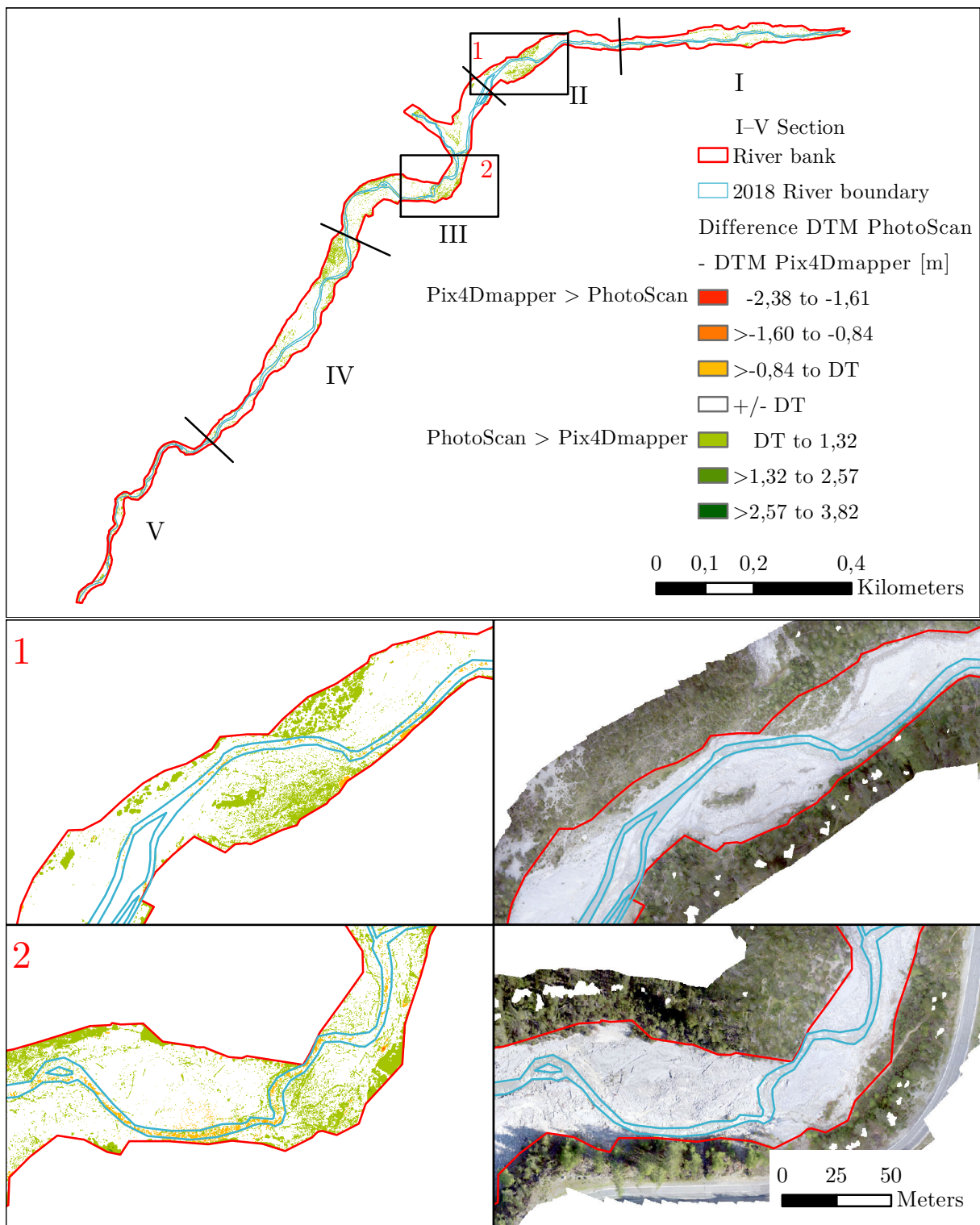


Figure 13: DoD PhotoScan-Pix4Dmapper (top) and 2 enlarged extracts (bottom-left) with corresponding orthofoto (bottom-right), 7.6 cm resolution (own depiction, data basis: own calculations, river bank and river boundary 2018)

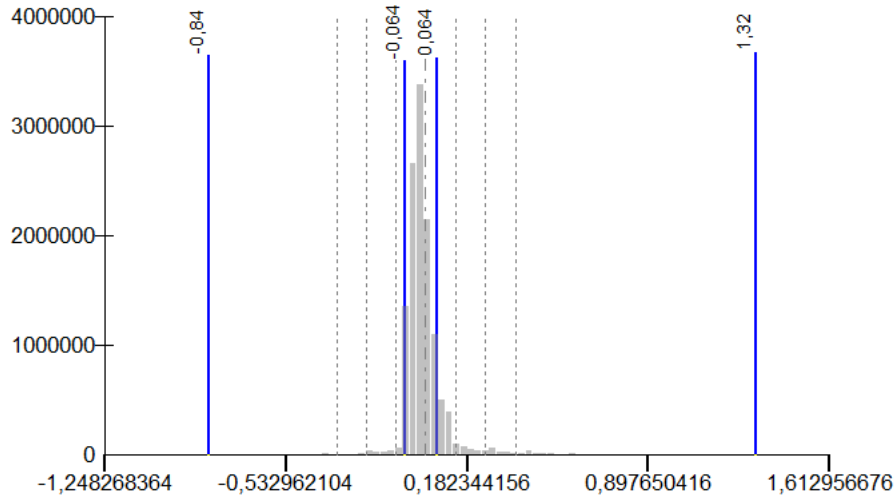


Figure 14: Histogram of the DoD PhotoScan-Pix4Dmapper [m] (screenshot from the classification properties of the DoD PhotoScan-Pix4Dmapper in ArcMap)

3.3 Change analysis 2003 – 2018

The change map of 2003 and 2009 displayed in figure 15 shows that changes occurred in all areas of the study object with more changes in the upper wider part (cf. sections I–IV) than in lower narrower part (cf. section V). Overall, the areas where there is a net loss of height and correspondingly of material (red and orange) outweigh those few where material was deposited (green) (cf. figure 15). The total numbers confirm the visual results. The total erosion is $7\,694.53\text{ m}^3$ whereas the total deposition is more than 22-fold smaller with 343.58 m^3 . Section III and IV account for most of the deposition with 162.33 m^3 (cf. section III) and 274.26 m^3 (cf. section IV). The biggest contribution to the erosion deliver section I with $2\,252.58\text{ m}^3$ and section III with $2\,457.78\text{ m}^3$ (cf. table 10).

Table 10: Volumetric changes [m^3] between 2003 and 2009 for the single sections and in total (own calculations)

Section	I	II	III	IV	V	Total
Erosion	-2 252.58	-942.62	-2 457.78	-1 247.36	-794.19	-7 694.53
Deposition	0.00	6.61	162.33	146.37	28.27	343.58
Net change	-2 252.58	-936.01	-2 295.45	-1 100.99	-765.92	-7 350.95

Taking a closer look at the map two kinds of loss can be distinguished within the sections. Smaller losses in the central part of the streambed as visible on enlargements 1 and 3 or major losses of between 1 m and 3 m at the sides of the stream banks (cf. enlargements 1–4).

The only bigger sections with a bigger win of material are in the area of the confluence – here more than 1 m (cf. enlargement 2) – and before the stream becomes narrower again (cf. enlargement 4). Here between 0.5 m and 1 m got deposited (cf. figure 15).

Taking a look at the changes between 2009 and 2018 figure 16 shows that the major changes occur in the upper four sections of the study object with smaller changes being present in section V. Here losses range up to 0.95 m and wins up to 1.39 m. The major changes can be separated into areas where there is mainly a deposit of material (cf. sections I and III) and areas where there is a loss (cf. sections II and IV). The biggest win of material occurs in the section of the confluence and further downstream (cf. section III). Here magnitudes of between 0.08 m and up to 4.26 m are reached. The losses are less severe and reach up to a maximum of 2.29 m. Erosion in the magnitude of more than 0.95 m can be observed mainly at the edges of the streambed (between enlargements 2 and 3, enlargement 3). Next to the elevation change the masked out stream is recognizable in all enlargements (cf. figure 16). In numbers there is a total net change of $13\,361.15\text{ m}^3$. Section III has the biggest positive contribution with a deposition of $14\,740.52\text{ m}^3$, sections II-IV all contribute with erosion of between 900 m^3 and $1\,550\text{ m}^3$ (cf. table 11).

Table 11: Volumetric changes [m^3] between 2009 and 2018 for the single sections and in total(own calculations)

Section	I	II	III	IV	V	Total
Erosion	-615.26	-935.78	-1 067.82	-1 533.21	-319.24	-4 471.31
Deposition	1 792.69	509.41	14 740.52	534.35	255.49	17 832.46
Net change	1 177.43	-426.37	13 672.70	-998.86	-63.75	13 361.15

Compared to the period before (2003–2009) the changes between 2009 and 2018 are ubiquitous and more distinct (cf. figures 15 and 16). Whereas for 2003–2009 in three sections a deposition smaller 30 m^3 can be noticed, in the period 2009–2018 the lowest value is around 250 m^3 . In the first period there is constant net loss for all sections of at least 750 m^3 , while in the second period sections with net win and lose alternate with one another until section V, where almost no net change can be observed (cf. tables 10 and 11). Furthermore, in the second period changes in the IV part of the stream were more recognizable and prominent (cf. figures 15 and 16). This differences can also be seen in the numbers. For 2003–2009 there is a net loss of around $7\,000\text{ m}^3$ and for 2009–2018 a win of more than $13\,000\text{ m}^3$ (cf. tables 10 and 11). Converted to an annually value a net change of around $-1\,225\text{ m}^3\text{ yr}^{-1}$ for the period 2003–2009 and around $1\,485\text{ m}^3\text{ yr}^{-1}$ for the period 2009–2018 is reached. Transferred to the area this means a net change of $-0.022\text{ m}^3\text{ m}^{-2}\text{ yr}^{-1}$ for 2003–2009 and $+0.027\text{ m}^3\text{ m}^{-2}\text{ yr}^{-1}$ for 2009–2018.

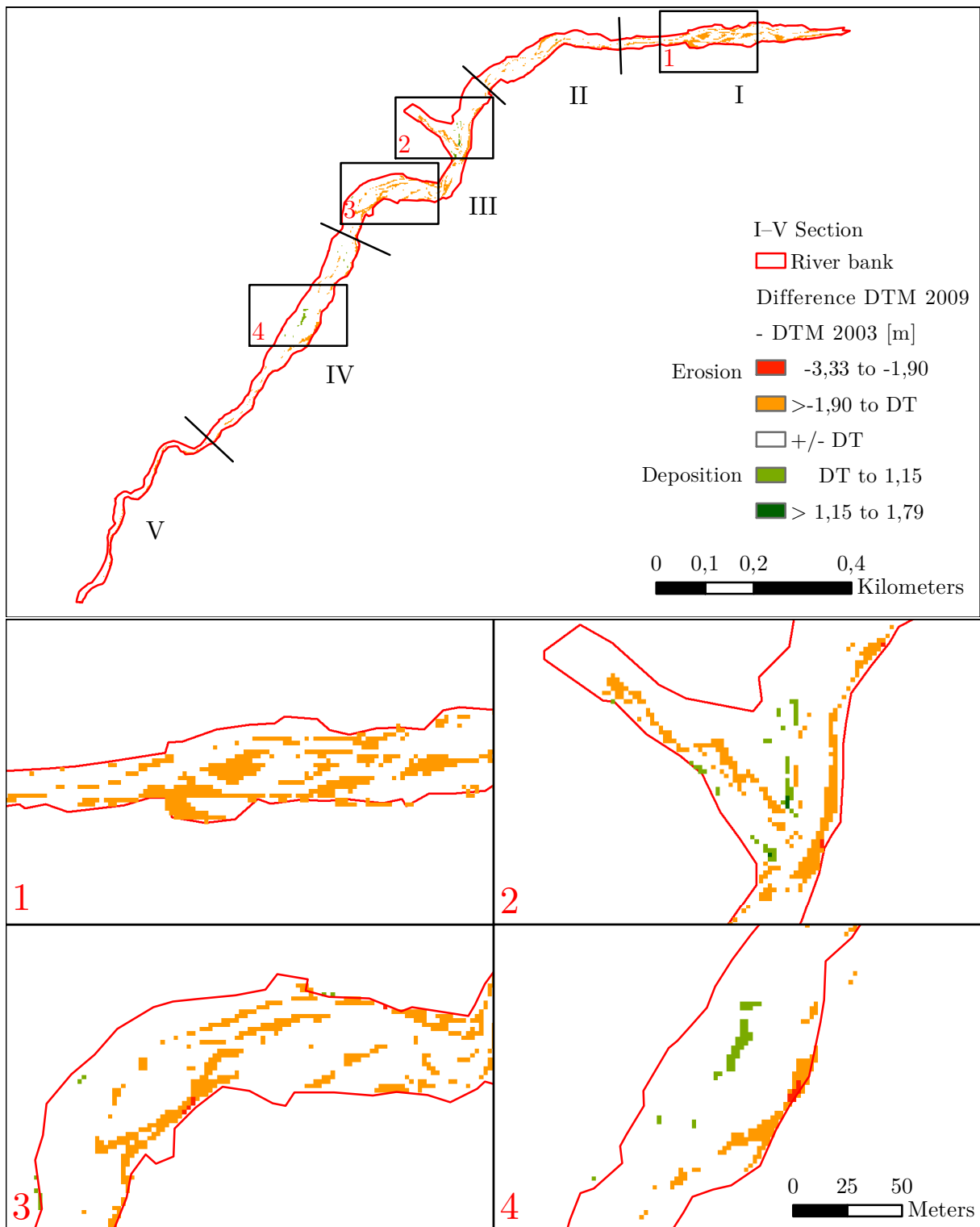


Figure 15: DoD 2009-2003 (top) and four enlarged extracts (bottom), 2 m resolution (own depiction, data basis: own calculations, river bank 2003/2009)

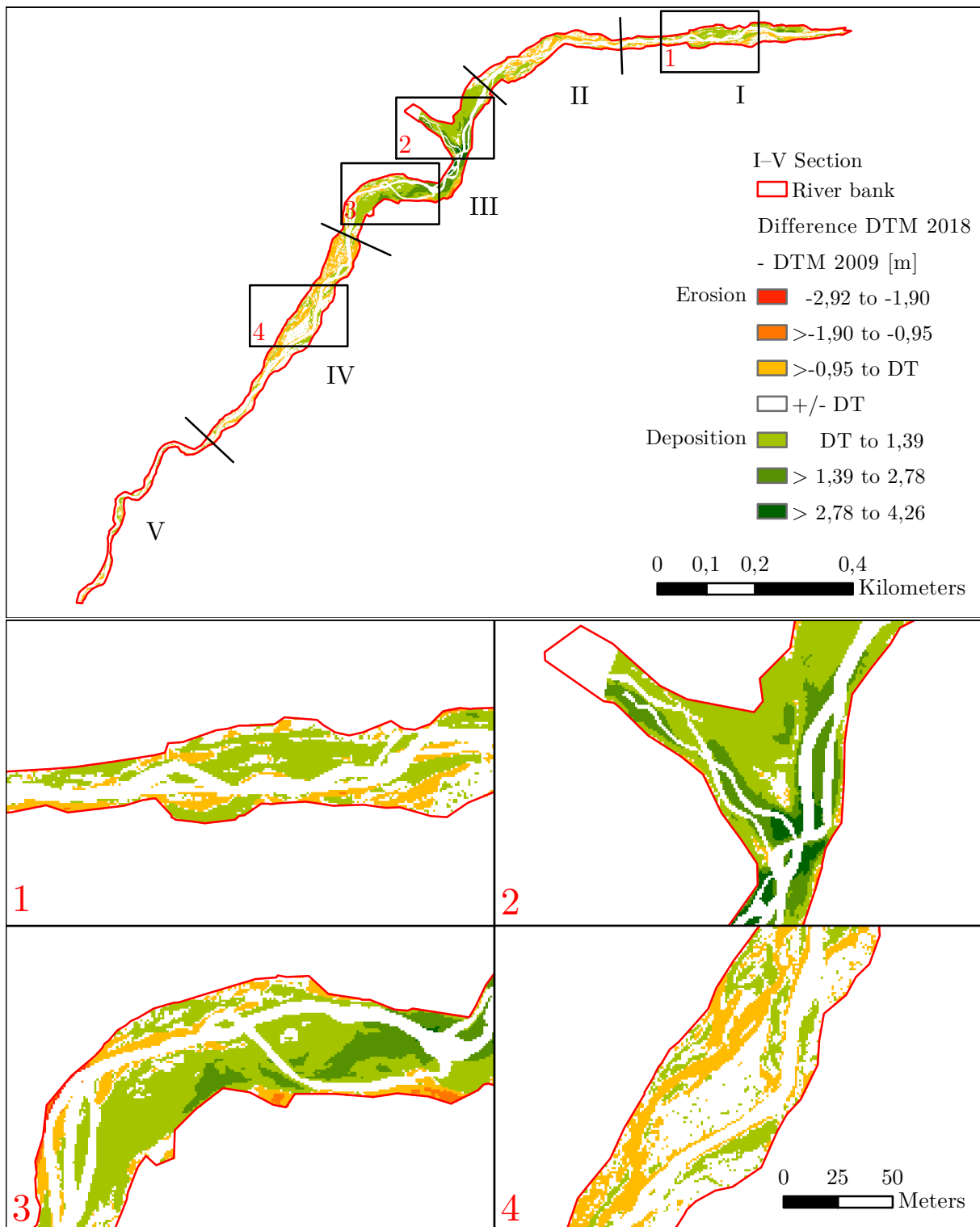


Figure 16: DoD 2018-2009 (top) and four enlarged extracts (bottom), 1 m resolution (own depiction, data basis: own calculations, river bank 2009/2018)

4 Discussion

4.1 Pix4Dmapper versus PhotoScan

4.1.1 Software properties and settings

Comparing the software properties and settings of both programmes the analysis showed that both have its advantages and disadvantages. The more detailed user manual in Pix4Dmapper can be seen as an advantage for easily finding the best software settings. Because it is not possible to test all different options due to time and technical limitations, it is very helpful to be able to draw on the experience and recommendation of the developers. When comparing the automation of the workflow it has to be mentioned that PhotoScan does offer the possibility of automating the whole process via a batch processing feature (cf. Chapter 7. Automation in Agisoft (2018)) but it is not the default way and more complex to implement than in Pix4Dmapper. Because in the end only one model was created with PhotoScan, the batch process was not further investigated.

Even though Pix4Dmapper offers an automatic point cloud classification, which saves a lot of time compared to finding the best parameters in PhotoScan, the automatic classification shows its downside in falsely classifying points. That also the Pix4D developers still see room for improvement is documented by the fact that the point cloud classification feature will be revised. In the future it will be possible for users to create their own training data for the point cloud classification algorithm and to choose between different classifiers (e.g. outside/inside study object) (Becker et al., 2017). Comparing the time needed for the point cloud classification in Pix4Dmapper, including the time needed for the post correction, with the time needed to find the best parameters in PhotoScan the automatic classification is still less time consuming. That an automatic classification is the future despite its problems becomes apparent when looking at PhotoScan's latest major software update. Since the update on the 31.12.2018 to version 1.5.0 an automatic multi-class point cloud classification coupled with a machine learning algorithm has been

implemented (Agisoft, n.y.). It will replace the currently time consuming trial and error process of finding the right parameters.

The theoretically reasonable approach of Pix4Dmapper to weight GCPs marked on a higher zoom level more causes doubts in practice. This is the case not only because the only mentioning of this non-suppressible behaviour is a clause in one of the Pix4D Academy videos (Pix4D, 2019a) but also as in practice sometimes an overexposed, blurry and unsure GCP can be better marked on a high zoom level. In the end it is not verifiable if the model quality was improved thanks to the GCP weighting or not.

That PhotoScan can export the DTM in GSD resolution is an advantage over Pix4Dmapper. Still it is important to keep in mind that when dealing with such high resolutions as in this work, where the GSD is smaller than the RMSE of the GCPs and the RMSE of the model quality, the DTM resolution suggests an accuracy that can not be met by the model because the input data does not allow for it. Thus, although it is technical possible to gather high resolution topography data, it is in the light of the research question not always advisable (Bangen et al., 2014). In addition higher resolution models are more complicated to handle and need more processing and storage space. Nevertheless, the export in a higher resolution is superior over a lower because the method can be controlled when the downsampling is taking place outside Pix4Dmapper or PhotoScan. That the downsampling method can have a significant effect on the final DTM is shown for example by Becek (2007), who compared the decimation downsampling method with the averaging downsampling method.

4.1.2 Processing time

When comparing the processing times it is important to keep in mind that both programmes execute the same tasks but group them differently. Thus not for all single tasks processing times are given in the processing reports and not all can be compared directly. Next to the different design of the programmes one explanation for this might be found in the automation. The automation can be both time-saver and -waster. Time-saver because the next task will always be conducted no matter if the user is present to start it or not, time-waster if, as in this work, the process hangs up and all previous steps of the workflow have to be executed again once the bug is noticed. The in total almost three times longer processing time in PhotoScan can be deceptive, because: for the initial processing in Pix4Dmapper no times are given and could not be included in table 3; the software version of PhotoScan that was available was released more than 2 years earlier than the one for Pix4Dmapper (cf. 2.3.1 Pix4Dmapper and PhotoScan); the dense point

cloud could be processed on a higher image scale, which is more time consuming (Agisoft, 2018). That despite the two different image scales a comparison of both model results is still valid can be justified by the fact that for Pix4Dmapper the developers state the full scale option, a usually not significantly better result (Pix4D, 2019b). With the latest major update at the end of December 2018 PhotoScan was able to cut the processing time until after the dense point cloud in half for a dataset similar to the one used in this work (Agisoft, n.y.). Overall one can say that if all settings are known, no matter if taken from the manuals or from own exploration on a smaller dataset, a study area of the size of this work can be conducted for both programmes in each two to three days. In this time included are tasks not timewise mentioned in the processing report, for example the identification of the GCPs, which depends on the amount of GCPs taken and the overlap of the pictures.

4.1.3 Model quality

Taking first only a look at the magnitude of the georeferencing error itself, regardless of the scenario and the programme, the RMSE and MAE are for all directions (X, Y and Z) below 0.08 m. These low values in the range of the GCP accuracy are proof that both programmes managed to correctly georeference the model independently from the amount of GCPs used for georeferencing (James and Robson, 2012). For Pix4Dmapper the difference between the 11 GCP scenario and the 42 GCP scenario is maximum 2 cm in one direction and thus below the GPS accuracy. Therefore, no negative effect could be noticed here when using more than the 5–10 GCPs recommended by Pix4D were used (Pix4D, 2017).

On a closer look the values of all four scenarios are in the range of similar works. Smith et al. (2014) come to MAEs of 0.04 m, 0.07 m and 0.05 m (X, Y and Z direction) and RMSEs of 0.05 m, 0.08 m and 0.05 m (X, Y, Z directions) using PhotoScan and 6 GCPs taken with a Differential Global Positioning System (DGPS) in a dry river bed environment. Dietrich (2016), who likewise used PhotoScan and 66 GCPs taken with a GPS in a riverscape, comes to lower RMSEs of 0.01 m, 0.02 m and 0.02 m (X, Y and Z directions).

Despite the three given examples from literature, where the georeferencing error is reported, this is not always done. Therefore, for Pix4Dmapper no corresponding values for stream/river environments could be found. One explanation for the omission of the georeferencing error could be that SfM-MVS was only the method used and the closer investigation of the used programmes was not the main objective in these works. Still it is advisable to report those errors, not only because it is easy to implement, since for

Pix4Dmapper the georeferencing RMSE and for PhotoScan the mean error ME are given in the processing report, but also because the best model is little meaningful if it is erroneously transferred to reality. That depending on the programme big errors can occur show for example Fonstad et al. (2013), who use the open-source programme JAG3D and come to georeferencing RMSEs of 0.44 m, 0.46 m and 0.19 m (X, Y and Z directions) for 10 GCPs in a bedrock channel floodplain.

Considering the validation of the model the results are in line with other works that recommend to use more GCPs for the georeferencing to obtain better results (cf. Agüera-Vega et al., 2017; Martínez-Carricondo et al., 2018). For the best result – the all scenario – the errors agree very well with the rule of thumb given by Ruzgienė et al. (2015) that the error in X and Y directions is in order of twice the GSD and in Z direction in order of three times.

Compared to similar study areas the values reached in this work for Pix4Dmapper and PhotoScan of 0.4 m for the $RMSE_z$ and 0.03 m MAE_z are 3 times (Smith et al., 2014), respectively five times (Javernick et al., 2014) lower. Javernick et al. (2014) come to a $RMSE_z$ of 0.23 m and an MAE_z of 0.16 m using 30 uniformly separated GCPs for georeferencing in a 1.6 km long braided river segment. Smith et al. (2014) reach 0.14 m for the $RMSE_z$ and 0.09 m for the MAE_z . An explanation for the higher values compared to this work could be that Javernick et al. (2014) included the water area, which is difficult to access and Smith et al. (2014) only used six GCPs for the georeferencing. Compared to the results of this work with 11 GCPs Javernick et al. (2014) come to lower and thus better accuracies.

In recent years increasingly more studies have realized the importance of the distribution and amount of GCPs for the error control in SfM-MVS (cf. Agüera-Vega et al., 2017; Martínez-Carricondo et al., 2018; Tahar, 2013). Still at the moment to the authors best knowledge there are non that do so in a river or stream environment. The work with a study area closest to the one here used is Tahar (2013), who investigated a 152 ha big protracted rectangle with an altitude difference of 60 m. He comes to errors of 0.3 m – 0.4 m (X, Y directions) and around 0.8 m (Z direction) for all scenarios from four up to nine GCPs tested. With that the error in the Z direction is similar to the one in this work achieved by PhotoScan for the quarter tmb scenario with 11 GCPs. Comparing this work's X and Y errors of the quarter tmb scenario to Tahar (2013) they are for both programmes in the order of 10s of centimetres lower and in Pix4Dmapper also the Z error is lower (cf. table 6). Following Martínez-Carricondo et al. (2018), who state the same for Tahar (2013), it can be conclude that the high values are due to the low number of GCPs. Other works that investigate the amount of GCPs come to the conclusion that 15 are as

good as 20 with X and Y errors of around 0.03 m and Z errors of around 0.05 m (Agüera-Vega et al., 2017). With that they are slightly better but in the range of the two 21 GCP scenarios from this work. For 10 GCPs Agüera-Vega et al. (2017) come to low errors in X and Y direction of 0.03 m and a good Z error of 0.07 m, thus having better results than the GCP 11 scenario. Because Agüera-Vega et al. (2017) used PhotoScan as well, and because the better results can not be explained with the software, one explanation could be the square shape of the research area, which might be easier to correctly georeference and model.

Martínez-Carricondo et al. (2018) tested five different distributions and 12 combinations of GCPs ranging from four to a maximum of 36. Even though results might be not completely comparable because of their square and twice as big study area with 17.64 ha, there are similarities to this work. Martínez-Carricondo et al. (2018) conclude that the best results are obtained if the GCPs are placed on the edges and inside the study area. Because of the long and narrow study object in this work the inside is at the same time also the edge of the width. Therefore, only the all scenario with 42 GCPs has GCPs on the edges and inside the study object. For both programmes the all scenario is the best and gives similar values as Martínez-Carricondo et al. (2018), who reached 0.05 m in horizontal and vertical accuracy.

The comparison to similar studies showed that the values achieved in this work are plausible and a higher amount of GCPs distributed at the edges and inside the study area give the best results. The difference between both programmes are really small and it can be said that the amount and distribution has a bigger influence in the order of 10s of centimetres. Still it is not always easy to compare one's own findings with literature, since the given frame (study area, GCP distribution, software etc.) is never exactly the same, not to mention the processing options that are never explicitly described. Some discrepancy between works might be explained due to that fact.

4.1.4 Software pricing

Comparing the pricing of both software programmes, PhotoScan has a rather cheap offer with its standard edition, which is deemed not useful for this and most other works because neither a DTM nor an orthofoto export is possible (Agisoft LLC, 2019). Compared to other commercial software the advantage of both programmes is that the professional edition includes a lifetime licence. Other commercial providers such as Autodesk with Recap Pro charge a yearly amount of around 400 € (Autodesk GmbH, 2019). On the other hand a price of over 3 000 € for a lifetime licence is not cheap. Therefore, before

purchasing a software it is always important to how long the software will be needed and which software updates in the different packages are included. PhotoScan is in the lifetime licence and also with its educational licence cheaper than Pix4Dmapper, which in combination with the twice as long trial time of 30 days can be seen as two reasons why PhotoScan is used so often in the geosciences. After all, 30 days are enough time to process a project if the processing steps are known and an appropriate computer is available.

4.2 DTMs from aerial photos using SfM-MVS

After the error metrics has revealed good results for both programmes for the all scenario, the visual validation can confirm that. The good results are closely linked not only to the amount but also to the quality of the taken GCPs (Lucieer et al., 2014). Therefore, one reason for the good results can be seen in the high accuracy with which the GCPs could be gathered. This is not always an easy task due to the complex terrain and often hard accessibility of study sites in mountain environments (Martínez-Carricondo et al., 2018). The problem of the method mentioned in many studies not being able to correctly identify terrain beneath vegetation (cf. Fonstad et al., 2013; Javernick et al., 2016; van Iersel et al., 2018) could also be observed in the densely vegetated parts above the streambed. Because these parts were not part of the study object, there was no need for a deeper investigation here. The few solitary trees within the study object could be well covered via the point cloud classification. One explanation could be that each tree was covered from all sides via the aerial photos and thus was well represented via the dense point cloud. One other point responsible for errors in the DTM is wind and changing lighting conditions (van Iersel et al., 2018). Because the aerial photos were taken on a windless day, wind can be excluded as a source of error for this work. Changing lighting conditions were present between the photos due to different daytime and the high trees above the streambed causing shadows on the streambed. How big the influence of the lighting on the error is, can not comprehensively be quantified but as the georeferencing error is almost the magnitude of the validation error (cf. table 8) it can be assumed to be relatively low.

With the example of the PhotoScan DTM with the 2.97 cm resolution it could be seen that it is possible to create DTMs on a low one-digit centimetre resolution. It is important to have in mind that this might not always be required or meaningful (Carrivick et al., 2016). Direct proof for this was the need to downsample the PhotoScan DTM to be able to compare it to the Pix4Dmapper DTM, which could only be exported in a lower resolution. The export and displaying of the PhotoScan DTM in this high resolution of

around the errors in X, Y and Z directions can be justified with the goal of testing the limits of both programmes. In addition, when dealing with a small study object of a few ha because in this work even a fine resolution of 2.97 m takes a reasonable amount of memory space (around 1 GB) and is fast downsampled (in Saga less than 1 minute). The advantages of downsampling the model in-house are the control of the downsampling method and being able to choose the required resolution and extend.

For further use of the model in the future and when comparing it to a new acquisition of the study area a resolution above the error threshold deems however useful. In any case attention has to be paid to the error of the model, which needs to be considered when choosing the resolution of the DTM export and when interpreting the results.

Taking a look at the added time of the data acquisition and processing, it can be said that the method is capable of producing high resolution DTMs within days, thus making short repetitions e.g. between major events achievable.

The DoD between PhotoScan and Pix4Dmapper revealed that although both works have similar low error metrics for the all scenario, the final DTMs differ in heights. Those differences can be grouped into two categories: One where Pix4Dmapper produced higher elevations than PhotoScan and vice versa. The part where PixDmapper has higher elevation values than PhotoScan is mostly within the stream. The differences here between both programmes confirm the findings of other works that the water cannot be reliably be reconstructed (Cook, 2017; Gómez-Gutiérrez et al., 2014; Javernick et al., 2016), consequently this reinforces the decision to leave out the stream part in the change detection analysis.

Outside the stream mainly PhotoScan produced higher values than Pix4Dmapper. The differences can be grouped in coherent patches and many small scattered points. As the coherent patches are linked to spares vegetation on the ground it can be concluded that at least the *point cloud classification* of one programme had problems with correctly identifying and removing all vegetation. Since there were no GCPs taken in those vegetated side parts of the stream bed it can not be said which or if both of the *point cloud classifications* had problems here. Since it is more likely that the elevation in those section has been overestimated because parts of trees were falsely classified as ground point, it can be assumed that the Pix4Dmapper DTM is closer to reality in those areas. The differences that are visible in form of scattered points might be explained due to both programmes using different disclosed algorithms for the identification and matching of keypoints in the SfM part of the method. For PhotoScan Mali and Kuiry (2018) report an algorithm similar to the Scale-invariant feature transform (SIFT), for Pix4Dmapper no details are

revealed by the developers about the implemented algorithms (Pix4D, 2019a). Overall it can be concluded—despite the described differences—that in most parts of the study object Pix4Dmapper and PhotoScan came within the DT to the same results. In the parts with differences those were either in the excluded part of the stream and as the histogram revealed overall of rather low magnitude.

4.3 Change analysis 2003–2018

In general it is important to mention that with the two DoDs only changes from 2003 to 2009 and from 2009 to 2018 can be quantified. Changes that occurred in between cannot be accounted for since they might have been overlaid by later changes. To minimize those compensating effects, higher sample intervals would be necessary (Williams, 2012). According to Rascher and Sass (2017), the best survey interval is in the order of the time between two major relocation events. Because the time interval for relocation events in remote mountain environments is hard to access (Harb et al., 2013), at least a new data acquisition after each major event can be recommended (Rascher and Sass, 2017). This means that the *Ova dal Fuorn* in this section is for the moment well captured because the last major event was in 2017 (ENPK, 2017). Accordingly, it can be assumed that the 2017 event accounts for the biggest changes in the period 2009–2018. How high these are precisely, however, can not be exactly quantified.

For the 2003–2009 DoD some changes—mainly erosion—can be observed but for the major part of the study object no conclusion can be drawn because the changes here are within the DT of ± 0.50 m. That such a high DT is not suitable is confirmed by Javernick et al. (2014), who consider errors of around 0.10 m as an adequate size for a change detection. In addition to the high DT the coarse resolution of 2 m further restricts a precise analysis. Despite these two limitations narrow protracted patterns in the changes could be observed. The most likely explanation for this can be seen in the flow behaviour of the stream. Taking a look at the volumetric change the deposition of 0 m^3 or almost 0 m^3 for the sections I, II and V is striking (cf. table 10). Because it is unlikely that there has been almost no deposition—especially in the confluence section where the *Ova da Val Ftur* delivers constantly new material—in six years, it can be assumed that a part of the actual deposition is below the DT and another part was cancelled out by erosion. The negative net changes for all sections reveal that a great amount of material was rinsed out of the study object. For more precise statements it would be necessary to research the sections on a higher interval.

For 2009–2018 a point for almost the whole study object can be made because of the low DT suitable for a change detection analysis (Javernick et al., 2014) and the fine resolution of 1 m. As a consequence the stream structure but also deposition and erosion in a “lineish“ form are clearly visible. The explanation for this form is artefactual and can be explained by the masked and during the calculation left out stream as well as material is more likely eroded and deposited on the sides of the stream. Looking at the absolute numbers (cf. table 11) the huge deposition in section III is remarkable. It can be assumed that the 2017 flood is responsible for the biggest part. On the one hand the *Ova da Val Ftur* brought a lot of material with the flood and when it dammed the *Ova dal Fuorn* all material usually transported by the stream could not flow further downstream. The accumulated material is most likely to be found upstream of the confluence. That all the material comes solely from the *Ova dal Fuorn* can be excluded because depositions of similar magnitude could not be found for the first period. In this section (III) the stream is still removing all the material that has been deposited here since 2009. In section IV the stream has the highest net erosion for the period. This shows that during the 2017 event either not a lot of material reached so far down or that most of it has already been eroded. Because the *Ova da Val Ftur* dammed the *Ova dal Fuorn* the theory that not a lot of material was deposited here seems more likely. Compared to section I–IV the stream has to flow faster in section V due to it’s narrow streambed. Consequently the channel has to be deeper, more pronounced, less meandering and less shifting. The high flow rate and the clear channel structure can be seen as an explanation for the low deposition and erosion values in this section.

Because each study has its own sampling interval and each side its distinct characteristic concerning the size, the relief, the geology and climate, a comparison of the absolute numbers is difficult (Rascher and Sass, 2017). Nevertheless, by comparing cubic metre per square metre per year at least the difference in size between study areas and the different sampling interval are taken into account. Therefore, this can help to check the values for credibility and allows for a rough placement. The results of this work with $-0.022 \text{ m}^3 \text{ m}^{-2} \text{ yr}^{-1}$ for 2003–2009 and $0.027 \text{ m}^3 \text{ m}^{-2} \text{ yr}^{-1}$ for 2009–2018 are in the same magnitude of other studies. Blasone et al. (2014), who investigated three sections of a small alpine mountain stream via DoDs out of terrestrial laser scanning DEMs found a few times higher values than this work for 2003–2009 of $-0.11 \text{ m}^3 \text{ m}^{-2} \text{ yr}^{-1}$, $-0.14 \text{ m}^3 \text{ m}^{-2} \text{ yr}^{-1}$ and $-0.23 \text{ m}^3 \text{ m}^{-2} \text{ yr}^{-1}$. The 2009–2018 value can be ranged between Lane et al. (2003), who come to a net change of $0.013 \text{ m}^3 \text{ m}^{-2} \text{ yr}^{-1}$ for a 1 km wide and 3.3 km long braided river section using DEMs out of digital photogrammetry, laser altimetry and image processing, and between Rascher and Sass (2017), who calculate $0.044 \text{ m}^3 \text{ m}^{-2} \text{ yr}^{-1}$ for tributary

trenches of an alpine river using multi-temporal terrestrial laser scanning.

The small deviation from other works can be explained with the study – and study sides specifics – already mentioned at the beginning. Rascher and Sass (2017) for example found that the net change is two times higher for a two-year period when adding the results of all surveys over the two years (four) compared to only taking the first and last. The DoD technique used here has therefore to be seen as lower limit for the changes (Williams, 2012) and small changes due to errors in the DEMs are not quantifiable (Brasington et al., 2003). To further improve the results the DT approach could be replaced by a more complex one even though the DT approach is widely used (Williams, 2012). Wheaton et al. (2009) suggest the use of a spatially variable model of elevation uncertainty based on a flexible and robust fuzzy inference system. Using that they were also able to capture low but meaningful changes and were successfully able to distinguish them from noise.

5 Conclusion

5.1 Implications

In this work SfM-MVS was used in two different programmes namely PhotoScan and Pix4Dmapper to create high resolution DTMs. During that process different settings of GCPs consisting of three different amounts (42, 21 (2x), 11) in three different distributions (full, tmb (2x), half) were compared for the first time in a longish research object. Comparing these two commercial software programmes was a new approach and had not been done so far.

The evaluation of the software properties and settings showed that both programmes have their strengths and weaknesses. PhotoScan for example has a good export of the GCP error but provides a simpler documentation. Pix4Dmapper has a very good documentation but enables the DTM export only in resolution of five times the GSD. Timewise Pix4Dmapper was superior over PhotoScan and enabled a faster processing in the compared versions. In terms of accuracy both managed to correctly georeference the model in all four GCP scenarios with PhotoScan being slightly inaccurate in the half tmb scenario with 21 GCPs. The validation showed that both programmes delivered good results for the all scenario, decent for the half uniform and the half tmb but weak for the quarter tmb. Pix4Dmapper had in two of the four scenarios marginally better results (all, half uniform) and in the quarter tmb clearly better results. The direct comparison of both DTMs via a DoD showed that, despite the good error metrics for both programmes, there were differences in the constructed DTMs. As those could be mainly linked to the vegetated parts, close attention needs to be paid to the *point cloud classification*. Comparing the price showed that Pix4Dmapper is more expensive than PhotoScan and that especially the educational version of PhotoScan is for researcher more attractive than Pix4Dmapper.

Taking all the investigated points into account, it can be concluded that neither software is clearly superior over the other and that both have their specific peculiarities. For users that require an automatic workflow that is easy to implement or only have the possibility of including few GCPs Pix4Dmapper can be recommended, for price sensitive users in the

educational/research field PhotoScan is the better option. Therefore, the first hypothesis, that PhotoScan is superior over Pix4Dmapper, can not be confirmed. Nevertheless, this work can be seen as a help to find the best option for the individual user when having to decide between those two commercial software programmes.

In general, comparing software in the highly active field of SfM-MVS is quite challenging because of the regular improvements and updates. Even if the two latest versions of the programmes would have been available at the beginning of this study – which was unfortunately not possible due to financial restrictions – the comparison would have already been outdated because in the meantime PhotoScan released a major update. Because the update is having an automated point cloud classification implemented, shorter local processing times and a cloud processing for extensive projects, further research will have to evaluate how the new possibilities will be accepted and applied by the software users. The comparison of the different GCPs scenarios showed that the scenario with the most GCPs spread equally over the whole study object delivered the best results. Following hypothesis 1, that a longish research object behaves in an analogue way to a squared considering different amounts and distributions of GCPs, can be confirmed.

In a second part of this work DoDs were deployed to come to a change analysis of the study object in the research period of 2003–2018. After a major rainfall event in 2017 the area changed significantly but had not been quantitatively researched so far. With the help of the DoDs it could be shown that the changes between 2009–2018 were more prominent than in the period before (2003–2009) and the biggest change can most likely be linked to the 2017 event. It could further be shown that the temporal and spatial resolutions as well as the magnitude of the error are limiting factors for the accuracy of the interpretation. Preferable options are here: acquisitions after each major event, 1 m spatial resolution or less and an error of around 0.10 m or lower. For the change analysis the DTM created from SfM-MVS proved to be more than sufficient. It had to be downsampled to be compared with the coarse LiDAR ones. SfM-MVS DTMs can therefore be a great help when investigating river/stream topography changes. Consequently hypothesis 3, that the 2017 event had a major impact on the channel topography and that changes during the second period were more severe than during the first, can be confirmed. Hypothesis 4, SfM-MVS DTMs are sufficient for change analysis, can be accepted.

5.2 Prospective

With Pix4Dmapper and PhotoScan this work was limited to two available commercial programmes. As these are not the only ones available (cf. PhotoModeler used by Micheletti et al. (2015) or Autodesk ReCap) a comprehensive study deems useful including the latest version of PhotoScan. Considering the price of each single programme, this is however not an inexpensive task. The error metrics for the validation used in this study and described in detail provide a good basis for future work and it is to be hoped that others will follow the in this work presented approach and include a sufficient description of the used metrics. Thus the validation of upcoming studies will become more comprehensible for everyone. Nevertheless, this work does not claim to be complete and more metrics such as the Mean Absolute Deviation (MAD) or Mean Error (ME) could be included (cf. Mali and Kuiry, 2018).

This work has done a first step in the investigation of the optimal amount and distribution of GCPs for SfM-MVS in a longish research object, but for a better assessment more variations in distribution and number of GCPs should be tested. A good example of a squared research area that could be applied to a longish can be found in Agüera-Vega et al. (2017). Implementing more repetitions of one number of GCP would have the advantage to also be able to calculate the mean deviation.

For the change analysis it will be possible to gain a detailed understanding of erosion and deposition patterns in a clearly higher resolution once a second acquisition of the area has been done. Since the method of the DT for the error assessment used here is a generous approach, for the new acquisition a more sophisticated one, like the one mentioned by Wheaton et al. (2009), is recommended.

Finally it can be said that for the future it is wise to focus on one of the 3 described areas (software, GCPs or change detection) to come to a deeper understanding not achievable by this kind of initial work.

All data used in this work was kindly provided by the SNP. The results of the calculations are stored by the SNP and can be looked at upon request.

6 References

- Agisoft, 2018. Agisoft PhotoScan User Manual: Professional Edition, Version 1.4. URL: https://www.agisoft.com/pdf/photoscan-pro_1_4_en.pdf. (Accessed 01.03.2019).
- Agisoft, n.y. Agisoft Metashape & Agisoft PhotoScan comparison: Try yourself and update for free. URL: https://www.agisoft.com/pdf/metashape_comparison.pdf. (Accessed 28.01.2019).
- Agisoft LLC, 2019. Metashape — photogrammetric processing of digital images and 3D spatial data generation. URL: <https://www.agisoft.com/>. (Accessed 09.03.2019).
- Agüera-Vega, F., Carvajal-Ramírez, F., Martínez-Carricondo, P., 2017. Assessment of photogrammetric mapping accuracy based on variation ground control points number using unmanned aerial vehicle. *Measurement* 98, 221–227. doi:10.1016/j.measurement.2016.12.002.
- Ascending Technologies GmbH, 2015. AscTec Falcon 8 + AscTec Trinity – Sicherheitsdatenblatt. URL: http://www.asctec.de/downloads/public/F8_AscTec-Falcon-8-AscTec-Trinity_Sicherheitsdatenblatt.pdf. (Accessed 18.01.2019).
- Autodesk GmbH, 2019. Abonnieren: ReCap Pro. URL: <https://www.autodesk.de/products/recap/subscribe?plc=RECAP&term=1-YEAR&support=ADVANCED&quantity=1>. (Accessed 01.05.2019).
- Bangen, S.G., Wheaton, J.M., Bouwes, N., Bouwes, B., Jordan, C., 2014. A methodological intercomparison of topographic survey techniques for characterizing wadeable streams and rivers. *Geomorphology* 206, 343–361. doi:10.1016/j.geomorph.2013.10.010.
- Becek, K., 2007. Comparison of Decimation and Averaging Methods of DEM's Resampling. doi:10.13140/2.1.1147.8088.
- Becker, C., Häni, N., Rosinskaya, E., d'Angelo, E., Strecha, C., 2017. Classification of Aerial Photogrammetric 3D Point Clouds. URL: <http://arxiv.org/pdf/1705.08374v1>. (Accessed 20.05.2019).

- Blasone, G., Cavalli, M., Marchi, L., Cazorzi, F., 2014. Monitoring sediment source areas in a debris-flow catchment using terrestrial laser scanning. *CATENA* 123, 23–36. doi:10.1016/j.catena.2014.07.001.
- Brasington, J., Langham, J., Rumsby, B., 2003. Methodological sensitivity of morphometric estimates of coarse fluvial sediment transport. *Geomorphology* 53, 299–316. doi:10.1016/S0169-555X(02)00320-3.
- BSF Swissphoto AG/SPM/DET, 2009. DTM und Orthophoto Ova Spin: Technischer Bericht.
- Bundesamt für Landestopografie swisstopo, 2010. SWISSIMAGE: Das digitale Farbornthophotomosaik der Schweiz. URL: https://www.swisstopo.admin.ch/content/swisstopo-internet/de/home/products/images/ortho/swissimage/_jcr_content/contentPar/tabs/items/dokumente/tabPar/downloadlist/downloadItems/588_1464190449870.download/infosi201003deu.pdf. (Accessed 18.04.2019).
- Bundesamt für Landestopografie swisstopo, 2012. swissALTI3D Ausgabebericht 2012. URL: https://shop.swisstopo.admin.ch/de/products/height_models/alti3D. (Accessed 10.04.2019).
- Bundesamt für Landestopografie swisstopo, 2018. swiss ALTI3D: Das hoch aufgelöste Terrainmodell der Schweiz.
- Carrivick, J.L., Smith, M.W., Quincey, D.J., 2016. Structure from Motion in the Geosciences: New Analytical Methods in Earth and Environmental Science. Wiley, Pondicherry (India).
- Cawood, A.J., Bond, C.E., Howell, J.A., Butler, R.W., Totake, Y., 2017. LiDAR, UAV or compass-clinometer? Accuracy, coverage and the effects on structural models. *Journal of Structural Geology* 98, 67–82. doi:10.1016/j.jsg.2017.04.004.
- Chai, T., Draxler, R.R., 2014. Root mean square error (RMSE) or mean absolute error (MAE)? – Arguments against avoiding RMSE in the literature. *Geoscientific Model Development* 7, 1247–1250. doi:10.5194/gmd-7-1247-2014.
- Chandler, J., Ashmore, P., Paola, C., Gooch, M., Varkaris, F., 2002. Monitoring river channel change using terrestrial oblique digital imagery and automated digital photogrammetry. *Annals of the Association of American Geographers* 92, 631–644.
- Chesley, J.T., Leier, A.L., White, S., Torres, R., 2017. Using unmanned aerial vehicles and structure-from-motion photogrammetry to characterize sedimentary outcrops: An

- example from the Morrison Formation, Utah, USA. *Sedimentary Geology* 354, 1–8. doi:10.1016/j.sedgeo.2017.03.013.
- Conrad, O., Bechtel, B., Bock, M., Dietrich, H., Fischer, E., Gerlitz, L., Wehberg, J., Wichmann, V., Böhner, J., 2015. System for Automated Geoscientific Analyses (SAGA) v. 2.1.4. *Geoscientific Model Development* 8, 1991–2007. doi:10.5194/gmd-8-1991-2015.
- Cook, K.L., 2017. An evaluation of the effectiveness of low-cost UAVs and structure from motion for geomorphic change detection. *Geomorphology* 278, 195–208. doi:10.1016/j.geomorph.2016.11.009.
- Dietrich, J.T., 2016. Riverscape mapping with helicopter-based Structure-from-Motion photogrammetry. *Geomorphology* 252, 144–157. doi:10.1016/j.geomorph.2015.05.008.
- Eidgenössische Nationalparkkommission ENPK Stiftung Schweizerischer Nationalpark Zerne, 2017. Schweizerischer Nationalpark Geschäftsbericht.
- Eltner, A., Baumgart, P., Maas, H.G., Faust, D., 2014. Multi-temporal UAV data for automatic measurement of rill and interrill erosion on loess soil. *Earth Surface Processes and Landforms* 40, 741–755. doi:10.1002/esp.3673.
- Environmental Systems Research Institute, 2015. ArcGIS Desktop.
- Fonstad, M.A., Dietrich, J.T., Courville, B.C., Jensen, J.L., Carbonneau, P.E., 2013. Topographic structure from motion: a new development in photogrammetric measurement. *Earth Surface Processes and Landforms* 38, 421–430. doi:10.1002/esp.3366.
- geo.admin.ch, 2019. Online Kartenservice des Bundesamt für Landestopografie KO-GIS (Koordination, Geoinformation und Services). URL: <https://s.geo.admin.ch/800d88e8f8>. (Accessed 12.02.2019).
- Gómez-Gutiérrez, Á., Schnabel, S., Berenguer-Sempere, F., Lavado-Contador, F., Rubio-Delgado, J., 2014. Using 3D photo-reconstruction methods to estimate gully headcut erosion. *CATENA* 120, 91–101. doi:10.1016/j.catena.2014.04.004.
- Haller, H., Eisenhut, A., Haller, R.M. (Eds.), 2014. Atlas des Schweizerischen Nationalparks: Die ersten 100 Jahre. volume 99/I of *Nationalpark-Forschung in der Schweiz*. 2., 2014 ed., Haupt Verlag, Bern.
- Harb, G., Schneider, J., Sass, O., Stangl, J., 2013. Sedimentfracht und Klimawandel in alpinen Einzugsgebieten (ClimCatch), in: Technische Universität Dresden, Institut für Wasserbau und technische Hydromechanik (Ed.), Technischer und organisatorischer

- Hochwasserschutz - Bauwerke, Anforderungen, Modelle. Dresden. Dresdner Wasserbauliche Mitteilungen, pp. 297–305.
- Hieber, M., 2018. *Analysis I*. 1. auflage 2018 ed., Springer, Berlin.
- James, M.R., Robson, S., 2012. Straightforward reconstruction of 3D surfaces and topography with a camera: Accuracy and geoscience application. *Journal of Geophysical Research: Earth Surface* 117, 1–17. doi:10.1029/2011JF002289.
- Jaud, M., Passot, S., Le Bivic, R., Delacourt, C., Grandjean, P., Le Dantec, N., 2016. Assessing the Accuracy of High Resolution Digital Surface Models Computed by PhotoScan® and MicMac® in Sub-Optimal Survey Conditions. *Remote Sensing* 8, 465. doi:10.3390/rs8060465.
- Javernick, L., Brasington, J., Caruso, B., 2014. Modeling the topography of shallow braided rivers using Structure-from-Motion photogrammetry. *Geomorphology* 213, 166–182. doi:10.1016/j.geomorph.2014.01.006.
- Javernick, L., Hicks, D.M., Measures, R., Caruso, B., Brasington, J., 2016. Numerical Modelling of Braided Rivers with Structure-from-Motion-Derived Terrain Models. *River Research and Applications* 32, 1071–1081. doi:10.1002/rra.2918.
- Kaiser, A., Neugirg, F., Rock, G., Müller, C., Haas, F., Ries, J., Schmidt, J., 2014. Small-Scale Surface Reconstruction and Volume Calculation of Soil Erosion in Complex Moroccan Gully Morphology Using Structure from Motion. *Remote Sensing* 6, 7050–7080. doi:10.3390/rs6087050.
- Lane, S.N., 2000. The Measurement of River Channel Morphology Using Digital Photogrammetry. *The Photogrammetric Record* 96, 937–961.
- Lane, S.N., Westaway, R.M., Murray Hicks, D., 2003. Estimation of erosion and deposition volumes in a large, gravel-bed, braided river using synoptic remote sensing. *Earth Surface Processes and Landforms* 28, 249–271. doi:10.1002/esp.483.
- Li, Z., Zhu, Q., Gold, C., 2005. *Digital terrain modeling: Principles and methodology*. CRC, Boca Raton, Fla.
- Lucieer, A., Turner, D., King, D.H., Robinson, S.A., 2014. Using an Unmanned Aerial Vehicle (UAV) to capture micro-topography of Antarctic moss beds. *International Journal of Applied Earth Observation and Geoinformation* 27, 53–62. doi:10.1016/j.jag.2013.05.011.

- Mali, V.K., Kuiry, S.N., 2018. Assessing the accuracy of high-resolution topographic data generated using freely available packages based on SfM-MVS approach. *Measurement* 124, 338–350. doi:10.1016/j.measurement.2018.04.043.
- Mancini, F., Dubbini, M., Gattelli, M., Stecchi, F., Fabbri, S., Gabbianelli, G., 2013. Using Unmanned Aerial Vehicles (UAV) for High-Resolution Reconstruction of Topography: The Structure from Motion Approach on Coastal Environments. *Remote Sensing* 5, 6880–6898. doi:10.3390/rs5126880.
- Martínez-Carricondo, P., Agüera-Vega, F., Carvajal-Ramírez, F., Mesas-Carrascosa, F.J., García-Ferrer, A., Pérez-Porras, F.J., 2018. Assessment of UAV-photogrammetric mapping accuracy based on variation of ground control points. *International Journal of Applied Earth Observation and Geoinformation* 72, 1–10. doi:10.1016/j.jag.2018.05.015.
- MeteoSchweiz, 2018a. IDAWEB: Niederschlagsdaten der Station Buffalora. URL: <https://gate.meteoswiss.ch/idaweb/login.do>. (Accessed 12.05.2019).
- MeteoSchweiz, 2018b. Klimanormwerte Buffalora: Normperiode 1981–2010. URL: https://www.meteoschweiz.admin.ch/product/output/climate-data/climate-diagrams-normal-values-station-processing/BUF/climsheet_BUF_np8110_d.pdf. (Accessed 12.05.2019).
- Micheletti, N., Chandler, J.H., Lane, S.N., 2015. Investigating the geomorphological potential of freely available and accessible structure-from-motion photogrammetry using a smartphone. *Earth Surface Processes and Landforms* 40, 473–486. doi:10.1002/esp.3648.
- Ouédraogo, M.M., Degré, A., Debouche, C., Lisein, J., 2014. The evaluation of unmanned aerial system-based photogrammetry and terrestrial laser scanning to generate DEMs of agricultural watersheds. *Geomorphology* 214, 339–355. doi:10.1016/j.geomorph.2014.02.016.
- Pix4D, 2017. Pix4Dmapper 4.1: User Manual. URL: <https://support.pix4d.com/hc/en-us/articles/204272989-Offline-Getting-Started-and-Manual-pdf->. (Accessed 01.03.2019).
- Pix4D, 2019a. Support. URL: <https://support.pix4d.com>. (Accessed 11.03.2019).
- Pix4D, 2019b. Tie points. URL: <https://support.pix4d.com/hc/en-us/articles/214483743>.
- Pix4D SA, 2019. Measure from images: A unique photogrammetry software suite for drone mapping. URL: <https://www.pix4d.com/>. (Accessed 09.03.2019).

- R Core Team, 2018. R: A Language and Environment for Statistical Computing. URL: <https://www.R-project.org/>.
- Rascher, E., Sass, O., 2017. Evaluating sediment dynamics in tributary trenches in an alpine catchment (Johnsbachtal, Austria) using multi-temporal terrestrial laser scanning. *Zeitschrift für Geomorphologie, Supplementary Issues* 61, 27–52. doi:10.1127/zfg_suppl/2016/0358.
- Ruzgienė, B., Berteška, T., Gečyte, S., Jakubauskienė, E., Aksamitauskas, V.Č., 2015. The surface modelling based on UAV Photogrammetry and qualitative estimation. *Measurement* 73, 619–627. doi:10.1016/j.measurement.2015.04.018.
- Sass, O., Harb, G., Truhetz, H., Stangl, J., Schneider, J., 2015. Abschlussbericht Projekt ClimCatch. Klimaund Energiefonds Projekt B175084. URL: https://static.uni-graz.at/fileadmin/urbi-institute/Geographie/pictures/misc/climcatch/Sass-et-al_ACRP4-ClimCatch_Endbericht.pdf. (Accessed 30.10.2018).
- Seitz, S.M., Curless, B., Diebel, J., Scharstein, D., Szeliski, R., 2006. A Comparison and Evaluation of Multi-View Stereo Reconstruction Algorithms, in: Fitzgibbon, A., Taylor, C.J., LeCun, Y. (Eds.), 2006 IEEE Computer Society Conference on Computer Vision and Pattern Recognition - Volume 1 (CVPR'06), IEEE. pp. 519–528. doi:10.1109/CVPR.2006.19.
- Smith, M.W., Carrivick, J.L., Hooke, J., Kirkby, M.J., 2014. Reconstructing flash flood magnitudes using ‘Structure-from-Motion’: A rapid assessment tool. *Journal of Hydrology* 519, 1914–1927. doi:10.1016/j.jhydrol.2014.09.078.
- Smith, M.W., Carrivick, J.L., Quincey, D.J., 2016. Structure from motion photogrammetry in physical geography. *Progress in Physical Geography* 40, 247–275. doi:10.1177/0309133315615805.
- Stumpf, A., Malet, J.P., Allemand, P., Pierrot-Deseilligny, M., Skupinski, G., 2015. Ground-based multi-view photogrammetry for the monitoring of landslide deformation and erosion. *Geomorphology* 231, 130–145. doi:10.1016/j.geomorph.2014.10.039.
- Tahar, K.N., 2013. An evaluation on different number of ground control points in unmanned aerial vehicle photogrammetric block. *ISPRS - International Archives of the Photogrammetry, Remote Sensing and Spatial Information Sciences XL-2/W2*, 93–98. doi:10.5194/isprsarchives-XL-2-W2-93-2013.
- Ullman, S., 1979. *Interpretation of Visual Motion*. MIT, Cambridge.

- USGS, n.y. Mapping, Remote Sensing, and Geospatial Data. URL: <https://www.usgs.gov/faqs/which-resampling-methods-are-best-preserving-dem-accuracy-and-terrain-characteristics>. (Accessed 11.04.2019).
- Uysal, M., Toprak, A.S., Polat, N., 2015. DEM generation with UAV Photogrammetry and accuracy analysis in Sahitler hill. *Measurement* 73, 539–543. doi:10.1016/j.measurement.2015.06.010.
- van Iersel, W., Straatsma, M., Addink, E., Middelkoop, H., 2018. Monitoring height and greenness of non-woody floodplain vegetation with UAV time series. *ISPRS Journal of Photogrammetry and Remote Sensing* 141, 112–123. doi:10.1016/j.isprsjprs.2018.04.011.
- Westoby, M.J., Brasington, J., Glasser, N.F., Hambrey, M.J., Reynolds, J.M., 2012. ‘Structure-from-Motion’ photogrammetry: A low-cost, effective tool for geoscience applications. *Geomorphology* 179, 300–314. doi:10.1016/j.geomorph.2012.08.021.
- Wheaton, J.M., Brasington, J., Darby, S.E., Sear, D.A., 2009. Accounting for uncertainty in DEMs from repeat topographic surveys: improved sediment budgets. *Earth Surface Processes and Landforms* 25, n/a–n/a. doi:10.1002/esp.1886.
- Williams, R.D., 2012. DEMs of Difference. *Geomorphological Techniques*, British Society for Geomorphology , 1–17.
- Willmott, C.J., Matsuura, K., 2005. Advantages of the mean absolute error (MAE) over the root mean square error (RMSE) in assessing average model performance. *Climate Research* 30, 79–82. doi:10.3354/cr030079.

Appendix

Digital appendix

Folder structure on the enclosed DVD (official University Tübingen versions)

- 01_Thesis_PDF
- 02_Latex-Files
- 03_R-work (GCP_error_import and Scripts)
- 04_DTMs
- 05_Orthofotos
- 06_DoDs
- 07_Processing_reports

For the SNP and the Research Committee of Swiss National Park versions

All data including a short description is stored on the sever of the SNP.

Processing reports

- Pix4Dmapper for the all scenario
- PhotoScan for the all scenario

- Important:** Click on the different icons for:
- Help to analyze the results in the Quality Report
 - Additional information about the sections

Click [here](#) for additional tips to analyze the Quality Report

Summary

Project	20180816_ovaDalFuorn_GCPs_set
Processed	2019-02-07 12:10:39
Camera Model Name(s)	NEX-7_16.0_6000x4000 (RGB)
Average Ground Sampling Distance (GSD)	1.53 cm / 0.60 in
Area Covered	0.233 km ² / 23.3375 ha / 0.09 sq. mi. / 57.6982 acres

Quality Check

Images	median of 80802 keypoints per image	
Dataset	636 out of 636 images calibrated (100%), all images enabled	
Camera Optimization	0.99% relative difference between initial and optimized internal camera parameters	
Matching	median of 19755.8 matches per calibrated image	
Georeferencing	yes, 42 GCPs (42 3D), mean RMS error = 0.026 m	

Preview

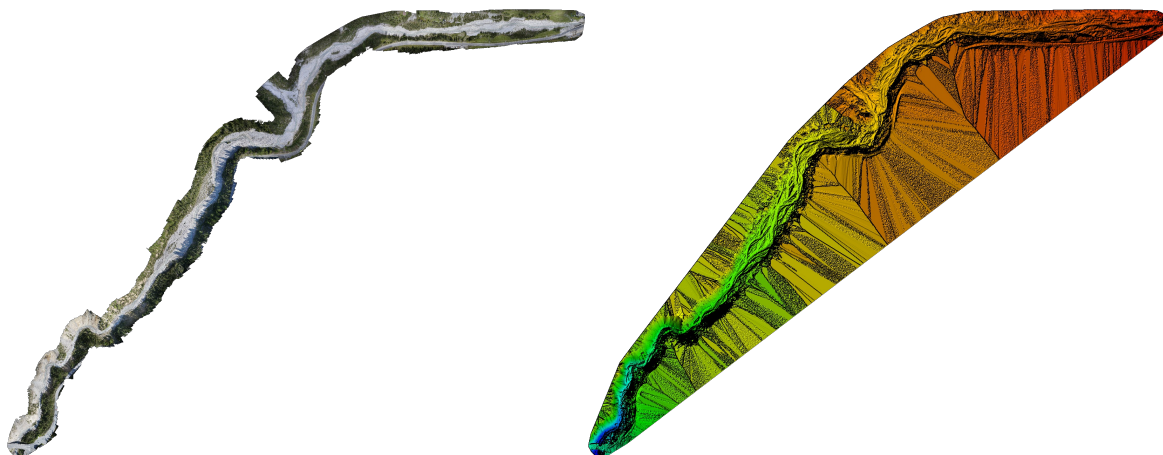


Figure 1: Orthomosaic and the corresponding sparse Digital Surface Model (DSM) before densification.

Calibration Details

Number of Calibrated Images	636 out of 636
Number of Geolocated Images	636 out of 636

Initial Image Positions

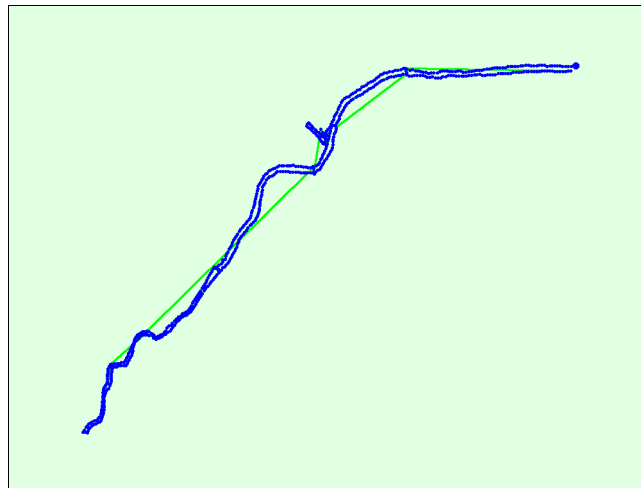
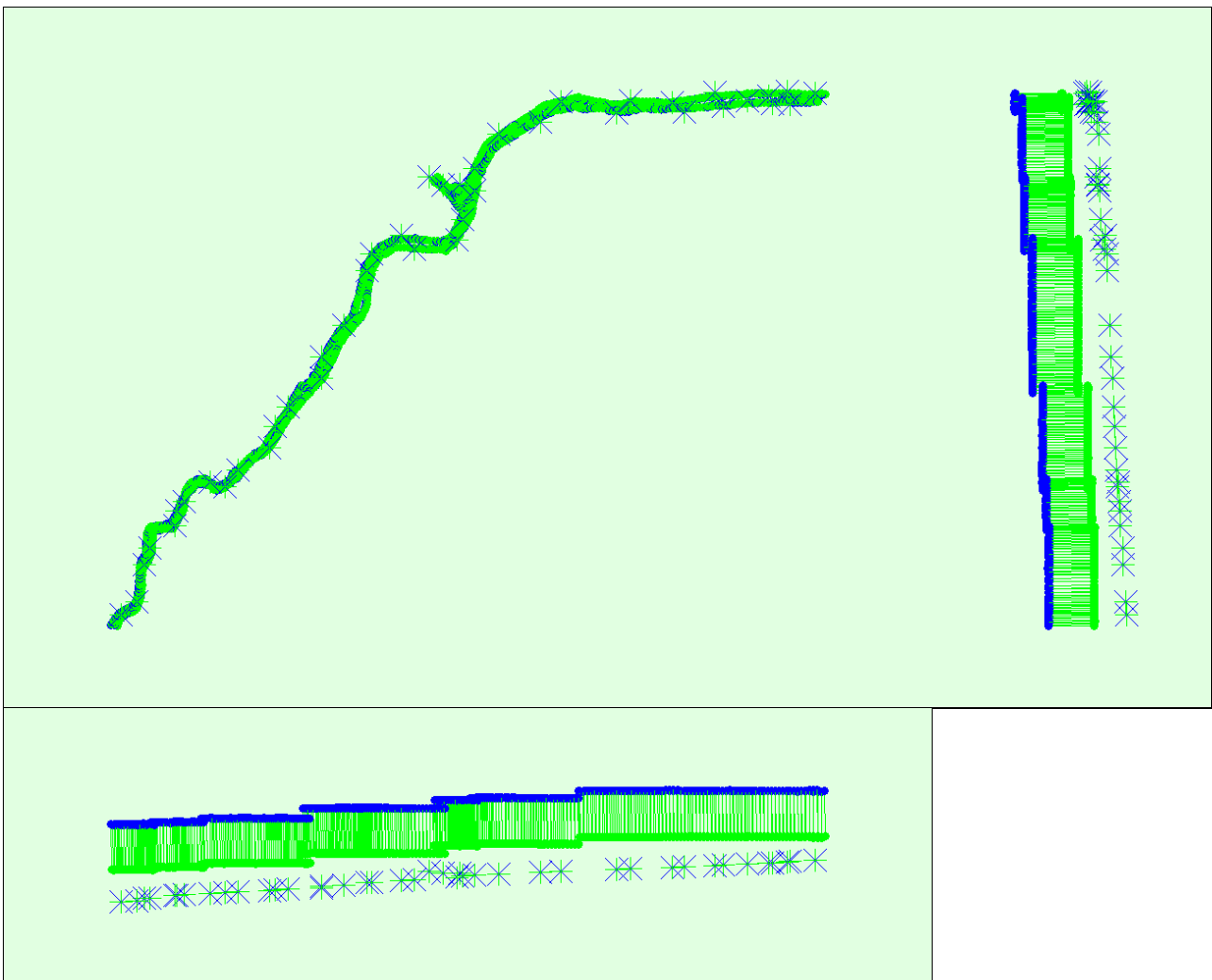


Figure 2: Top view of the initial image position. The green line follows the position of the images in time starting from the large blue dot.

Computed Image/GCPs/Manual Tie Points Positions



Uncertainty ellipses 100x magnified

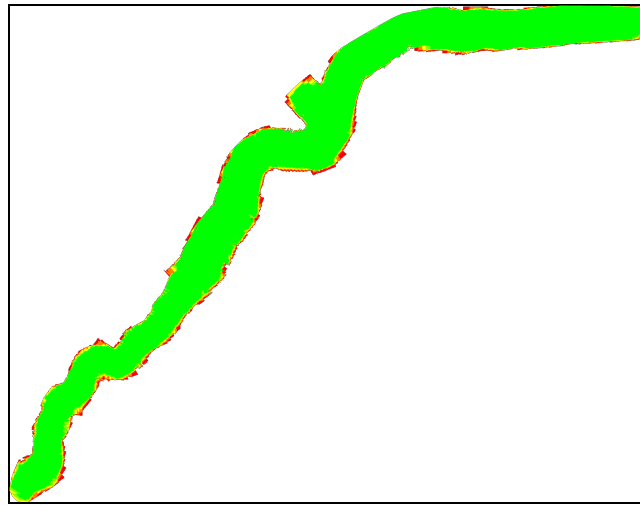
Figure 3: Offset between initial (blue dots) and computed (green dots) image positions as well as the offset between the GCPs initial positions (blue crosses) and their computed positions (green crosses) in the top-view (XY plane), front-view (XZ plane), and side-view (YZ plane). Dark green ellipses indicate the absolute position uncertainty of the bundle block adjustment result.

Absolute camera position and orientation uncertainties



	X[m]	Y[m]	Z[m]	Omega [degree]	Phi [degree]	Kappa [degree]
Mean	0.012	0.011	0.010	0.009	0.010	0.003
Sigma	0.003	0.002	0.001	0.002	0.003	0.001

Overlap



Number of overlapping images: 1 2 3 4 5+

Figure 4: Number of overlapping images computed for each pixel of the orthomosaic. Red and yellow areas indicate low overlap for which poor results may be generated. Green areas indicate an overlap of over 5 images for every pixel. Good quality results will be generated as long as the number of keypoint matches is also sufficient for these areas (see Figure 5 for keypoint matches).

Bundle Block Adjustment Details



Number of 2D Keypoint Observations for Bundle Block Adjustment	12666875
Number of 3D Points for Bundle Block Adjustment	3862149
Mean Reprojection Error [pixels]	0.164

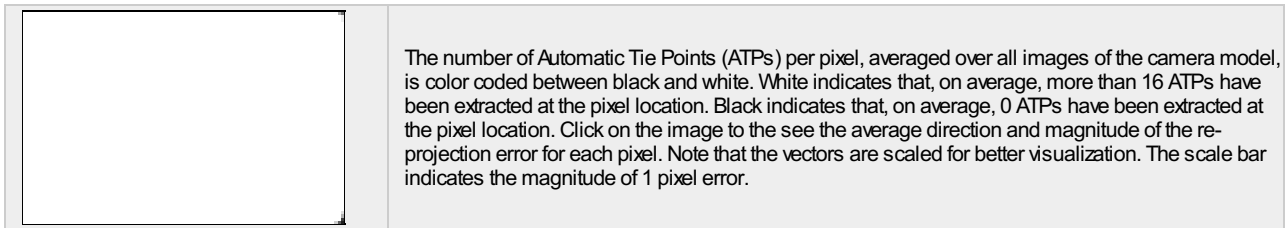
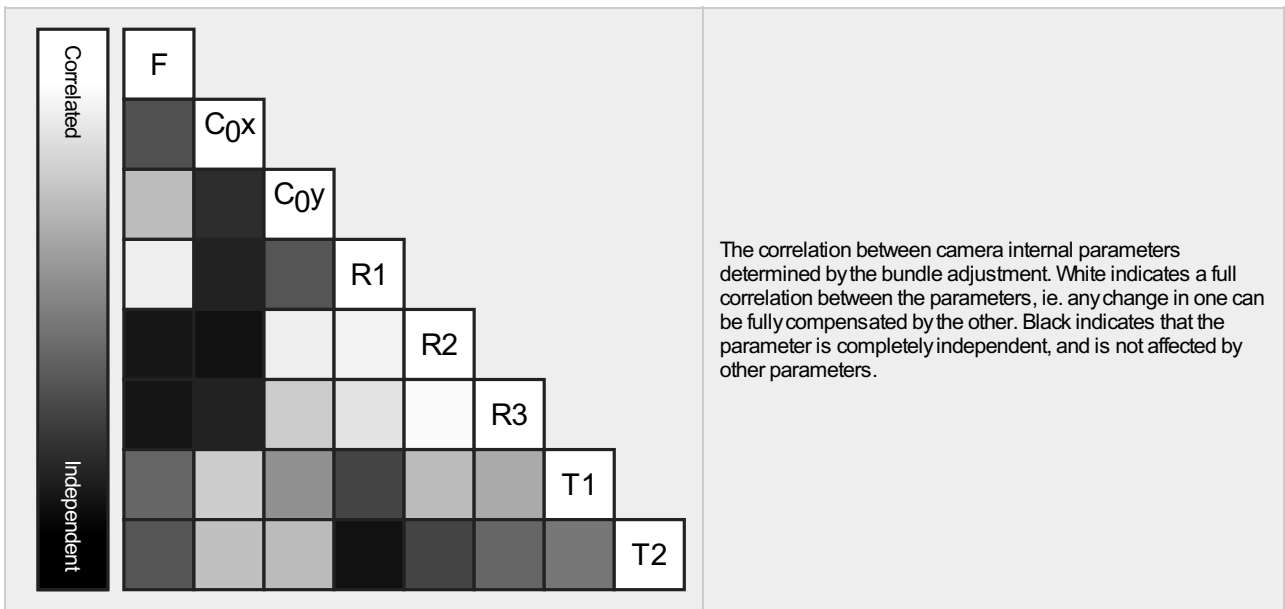
Internal Camera Parameters

NEX-7_16.0_6000x4000 (RGB). Sensor Dimensions: 36.000 [mm] x 24.000 [mm]



EXIF ID: NEX-7_E16mmF2.8_16.0_6000x4000

	Focal Length	Principal Point x	Principal Point y	R1	R2	R3	T1	T2
Initial Values	4051.370 [pixel] 24.308 [mm]	3000.000 [pixel] 18.000 [mm]	2000.000 [pixel] 12.000 [mm]	0.000	0.000	0.000	0.000	0.000
Optimized Values	4091.734 [pixel] 24.550 [mm]	2981.542 [pixel] 17.889 [mm]	1980.504 [pixel] 11.883 [mm]	-0.005	0.007	-0.004	0.000	0.001
Uncertainties (Sigma)	0.566 [pixel] 0.003 [mm]	0.093 [pixel] 0.001 [mm]	0.147 [pixel] 0.001 [mm]	0.000	0.000	0.000	0.000	0.000



2D Keypoints Table

	Number of 2D Keypoints per Image	Number of Matched 2D Keypoints per Image
Median	80802	19756
Mn	54726	164
Max	90795	32132
Mean	80340	19916

3D Points from 2D Keypoint Matches

	Number of 3D Points Observed
In 2 Images	2118460
In 3 Images	748305
In 4 Images	359937
In 5 Images	201723
In 6 Images	127031
In 7 Images	86032
In 8 Images	59236
In 9 Images	41559
In 10 Images	30235
In 11 Images	22252
In 12 Images	17182
In 13 Images	13434
In 14 Images	10982
In 15 Images	8472
In 16 Images	5984
In 17 Images	3562
In 18 Images	2554
In 19 Images	1707
In 20 Images	1004
In 21 Images	651
In 22 Images	441
In 23 Images	285

In 24 Images	245
In 25 Images	170
In 26 Images	158
In 27 Images	108
In 28 Images	100
In 29 Images	55
In 30 Images	66
In 31 Images	52
In 32 Images	36
In 33 Images	33
In 34 Images	30
In 35 Images	29
In 36 Images	14
In 37 Images	14
In 38 Images	7
In 39 Images	4

2D Keypoint Matches

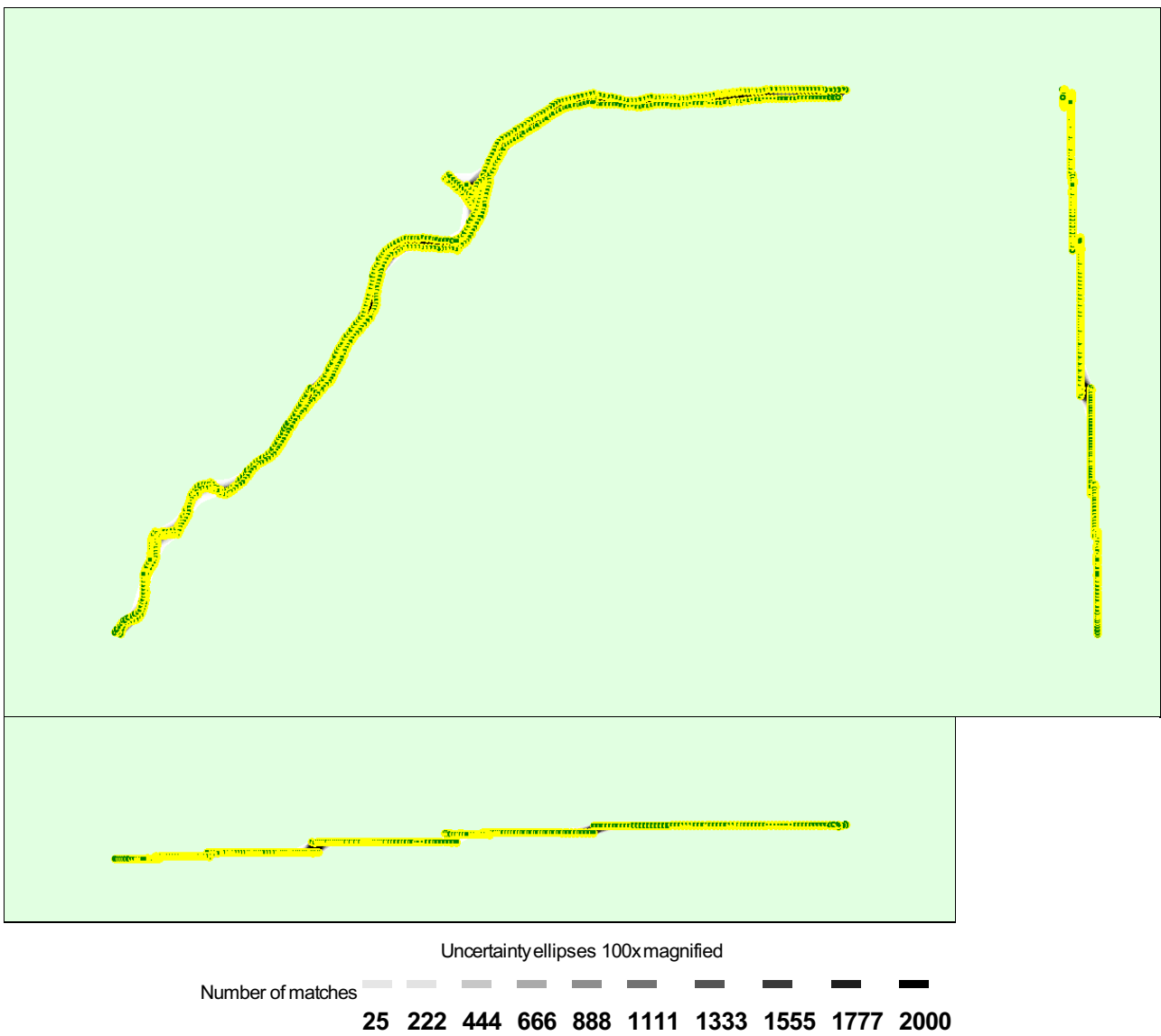


Figure 5: Computed image positions with links between matched images. The darkness of the links indicates the number of matched 2D keypoints between the images. Bright links indicate weak links and require manual tie points or more images. Dark green ellipses indicate the relative camera position uncertainty of the bundle block adjustment result.

Relative camera position and orientation uncertainties

	X[m]	Y[m]	Z[m]	Omega [degree]	Phi [degree]	Kappa [degree]
--	------	------	------	----------------	--------------	----------------

Mean	0.026	0.024	0.023	0.025	0.023	0.008
Sigma	0.006	0.009	0.007	0.009	0.008	0.002

Geolocation Details



Ground Control Points



GCP Name	Accuracy XY/Z [m]	Error X [m]	Error Y [m]	Error Z [m]	Projection Error [pixel]	Verified/Marked
2 (3D)	0.020/0.020	0.024	0.007	-0.009	0.819	16 / 16
4 (3D)	0.020/0.020	-0.097	-0.249	0.018	0.880	16 / 16
5 (3D)	0.020/0.020	0.031	0.027	0.058	0.846	14 / 14
6 (3D)	0.020/0.020	0.031	-0.003	0.033	0.779	14 / 14
8 (3D)	0.020/0.020	-0.007	-0.006	-0.039	0.907	12 / 12
9a (3D)	0.020/0.020	-0.011	-0.014	0.006	0.761	9 / 9
11 (3D)	0.020/0.020	-0.009	-0.000	0.026	1.064	13 / 13
12 (3D)	0.020/0.020	-0.008	0.004	-0.055	1.153	13 / 13
14 (3D)	0.020/0.020	-0.030	-0.025	-0.018	0.904	15 / 15
16 (3D)	0.020/0.020	-0.014	0.021	0.010	0.665	16 / 16
18 (3D)	0.020/0.020	-0.002	-0.010	0.018	0.701	17 / 17
21 (3D)	0.020/0.020	-0.010	-0.005	-0.025	0.749	15 / 15
23 (3D)	0.020/0.020	0.007	-0.005	0.010	0.619	18 / 18
24 (3D)	0.020/0.020	-0.000	0.014	-0.009	0.768	17 / 17
26 (3D)	0.020/0.020	-0.005	-0.015	-0.003	0.982	15 / 15
28 (3D)	0.020/0.020	0.011	-0.013	0.036	1.182	19 / 19
29 (3D)	0.020/0.020	-0.004	0.007	0.009	0.827	35 / 35
31 (3D)	0.020/0.020	-0.002	-0.001	-0.043	0.915	39 / 39
32 (3D)	0.020/0.020	0.000	0.011	0.015	1.035	17 / 17
33 (3D)	0.020/0.020	-0.004	0.007	0.012	1.068	6 / 6
36 (3D)	0.020/0.020	0.008	-0.003	0.021	1.278	19 / 19
38 (3D)	0.020/0.020	0.001	0.011	0.011	0.998	15 / 15
39 (3D)	0.020/0.020	-0.009	-0.001	-0.017	0.951	12 / 12
41 (3D)	0.020/0.020	0.007	-0.003	0.011	0.827	15 / 15
42 (3D)	0.020/0.020	0.002	-0.011	0.001	0.960	16 / 16
45 (3D)	0.020/0.020	0.004	0.012	-0.024	0.723	18 / 18
47 (3D)	0.020/0.020	-0.010	0.003	0.015	0.713	21 / 21
48 (3D)	0.020/0.020	-0.000	-0.017	0.002	0.632	23 / 23
50 (3D)	0.020/0.020	0.001	0.002	-0.001	0.728	16 / 16
51 (3D)	0.020/0.020	-0.003	0.005	-0.002	0.726	16 / 16
52 (3D)	0.020/0.020	-0.001	0.002	-0.003	0.795	15 / 15
54 (3D)	0.020/0.020	-0.001	-0.004	-0.002	0.814	16 / 16
55 (3D)	0.020/0.020	0.014	0.007	-0.007	1.008	17 / 17
56 (3D)	0.020/0.020	-0.008	-0.002	0.010	0.708	25 / 25
58 (3D)	0.020/0.020	0.014	-0.029	0.027	1.109	17 / 17
59 (3D)	0.020/0.020	-0.010	0.027	-0.026	0.946	23 / 23
60 (3D)	0.020/0.020	-0.017	0.015	0.008	0.989	19 / 19
62 (3D)	0.020/0.020	0.016	-0.016	0.008	1.052	25 / 25
63 (3D)	0.020/0.020	0.016	-0.001	-0.028	0.901	21 / 21
65b (3D)	0.020/0.020	-0.022	0.014	0.007	0.950	20 / 20
66 (3D)	0.020/0.020	0.003	-0.011	0.006	1.177	20 / 20
35 (3D)	0.020/0.020	-0.002	0.002	-0.012	0.997	20 / 20
Mean [m]		-0.002340	-0.005867	0.001309		
Sigma [m]		0.019298	0.039860	0.021723		
RMS Error [m]		0.019439	0.040289	0.021762		

0 out of 21 check points have been labeled as inaccurate.

Check Point Name	Accuracy XY/Z [m]	Error X [m]	Error Y [m]	Error Z [m]	Projection Error [pixel]	Verified/Marked
------------------	-------------------	-------------	-------------	-------------	--------------------------	-----------------

3		0.0323	0.0564	0.0216	1.0921	16 / 16
7		0.0243	0.0285	0.0060	1.0340	13 / 13
13		0.0106	0.0003	-0.0122	0.9811	14 / 14
15		-0.0047	-0.0055	0.0577	0.8935	16 / 16
17		0.0022	0.0111	0.0432	1.3229	16 / 16
19		-0.0346	0.0227	0.0564	1.0770	20 / 20
20		-0.0265	0.0095	0.0564	0.8829	19 / 19
22		-0.0205	0.0061	0.0269	0.9632	15 / 15
25		-0.0010	0.0046	0.0550	0.8751	17 / 17
27		-0.0146	-0.0030	0.0030	0.8187	20 / 20
30		-0.0122	0.0019	0.0212	0.8165	28 / 28
37		0.0139	0.0075	-0.0598	2.3580	24 / 24
40		-0.0027	-0.0232	-0.0052	1.0527	17 / 17
43		-0.0028	-0.0351	0.0919	0.8803	19 / 19
44		-0.0112	-0.0051	0.0664	0.9650	17 / 17
46		0.0031	-0.0105	-0.0070	0.7455	18 / 18
49		0.0001	0.0014	-0.0514	0.9164	24 / 24
53		0.0094	0.0104	-0.0420	0.6071	14 / 14
57		-0.0121	-0.0029	-0.0146	0.6546	27 / 27
61		0.0199	-0.0107	-0.0114	1.0249	25 / 25
64		-0.0150	0.0056	-0.0182	0.9230	21 / 21
Mean [m]		-0.002008	0.003327	0.013520		
Sigma [m]		0.016286	0.018014	0.040329		
RMS Error [m]		0.016409	0.018318	0.042535		

Localisation accuracy per GCP and mean errors in the three coordinate directions. The last column counts the number of calibrated images where the GCP has been automatically verified vs. manually marked.

🔍 Absolute Geolocation Variance



Min Error [m]	Max Error [m]	Geolocation Error X [%]	Geolocation Error Y [%]	Geolocation Error Z [%]
-	-15.00	0.00	0.00	0.00
-15.00	-12.00	0.00	0.00	0.00
-12.00	-9.00	0.00	0.00	0.00
-9.00	-6.00	0.00	0.00	0.00
-6.00	-3.00	0.00	0.00	0.00
-3.00	0.00	48.90	48.74	55.35
0.00	3.00	51.10	51.26	44.65
3.00	6.00	0.00	0.00	0.00
6.00	9.00	0.00	0.00	0.00
9.00	12.00	0.00	0.00	0.00
12.00	15.00	0.00	0.00	0.00
15.00	-	0.00	0.00	0.00
Mean [m]		-0.947060	-0.341956	100.025881
Sigma [m]		0.734734	1.006859	1.097297
RMS Error [m]		1.198648	1.063343	100.031899

Min Error and Max Error represent geolocation error intervals between -1.5 and 1.5 times the maximum accuracy of all the images. Columns X, Y, Z show the percentage of images with geolocation errors within the predefined error intervals. The geolocation error is the difference between the initial and computed image positions. Note that the image geolocation errors do not correspond to the accuracy of the observed 3D points.

Geolocation Bias	X	Y	Z
Translation [m]	-0.947060	-0.341956	100.025881

Bias between image initial and computed geolocation given in output coordinate system.

Relative Geolocation Variance



Relative Geolocation Error	Images X [%]	Images Y [%]	Images Z [%]
[-1.00, 1.00]	100.00	100.00	100.00
[-2.00, 2.00]	100.00	100.00	100.00
[-3.00, 3.00]	100.00	100.00	100.00
Mean of Geolocation Accuracy [m]	5.000000	5.000000	10.000000
Sigma of Geolocation Accuracy [m]	0.000000	0.000000	0.000000

Images X, Y, Z represent the percentage of images with a relative geolocation error in X, Y, Z.

Initial Processing Details



System Information



Hardware	CPU: Intel(R) Core(TM) i7 CPU 980 @ 3.33GHz RAM: 48GB GPU: NMDIA GeForce GTX580 (Driver: 23.21.13.9135)
Operating System	Windows 10 Enterprise, 64-bit

Coordinate Systems



Image Coordinate System	WGS 84 (EGM96 Geoid)
Ground Control Point (GCP) Coordinate System	CH1903+ / LV95 (-47m)
Output Coordinate System	CH1903+ / LV95 (-47m)

Processing Options



Detected Template	No Template Available
Keypoints Image Scale	Full, Image Scale: 1
Advanced: Matching Image Pairs	Aerial Grid or Corridor
Advanced: Matching Strategy	Use Geometrically Verified Matching: no
Advanced: Keypoint Extraction	Targeted Number of Keypoints: Automatic
Advanced: Calibration	Calibration Method: Standard Internal Parameters Optimization: All External Parameters Optimization: All Rematch: Auto, no

Point Cloud Densification details



Processing Options



Image Scale	multiscale, 1/2 (Half image size, Default)
Point Density	Optimal
Minimum Number of Matches	3
3D Textured Mesh Generation	yes
3D Textured Mesh Settings:	Resolution: Medium Resolution (default) Color Balancing: no
LOD	Generated: no
Advanced: 3D Textured Mesh Settings	Sample Density Divider: 1
Advanced: Image Groups	group1
Advanced: Use Processing Area	yes
Advanced: Use Annotations	yes
Time for Point Cloud Densification	02h:43m:03s

Time for Point Cloud Classification	15m:03s
Time for 3D Textured Mesh Generation	20m:50s

Results



Number of Generated Tiles	3
Number of 3D Densified Points	93606940
Average Density (per m ³)	689.41

DSM, Orthomosaic and Index Details



Processing Options



DSM and Orthomosaic Resolution	1 x GSD (1.53 [cm/pixel])
DSM Filters	Noise Filtering: yes Surface Smoothing: yes, Type: Sharp
Raster DSM	Generated: yes Method: Inverse Distance Weighting Merge Tiles: yes
Orthomosaic	Generated: yes Merge Tiles: yes GeoTIFF Without Transparency: no Google Maps Tiles and KML: no
Raster DTM	Generated: yes Merge Tiles: yes
DTM Resolution	5 x GSD (1.53 [cm/pixel])
Time for DSM Generation	01h:34m:58s
Time for Orthomosaic Generation	01h:49m:21s
Time for DTM Generation	02h:26m:29s
Time for Contour Lines Generation	00s
Time for Reflectance Map Generation	00s
Time for Index Map Generation	00s

GCP_all

Processing Report
10 February 2019



Survey Data

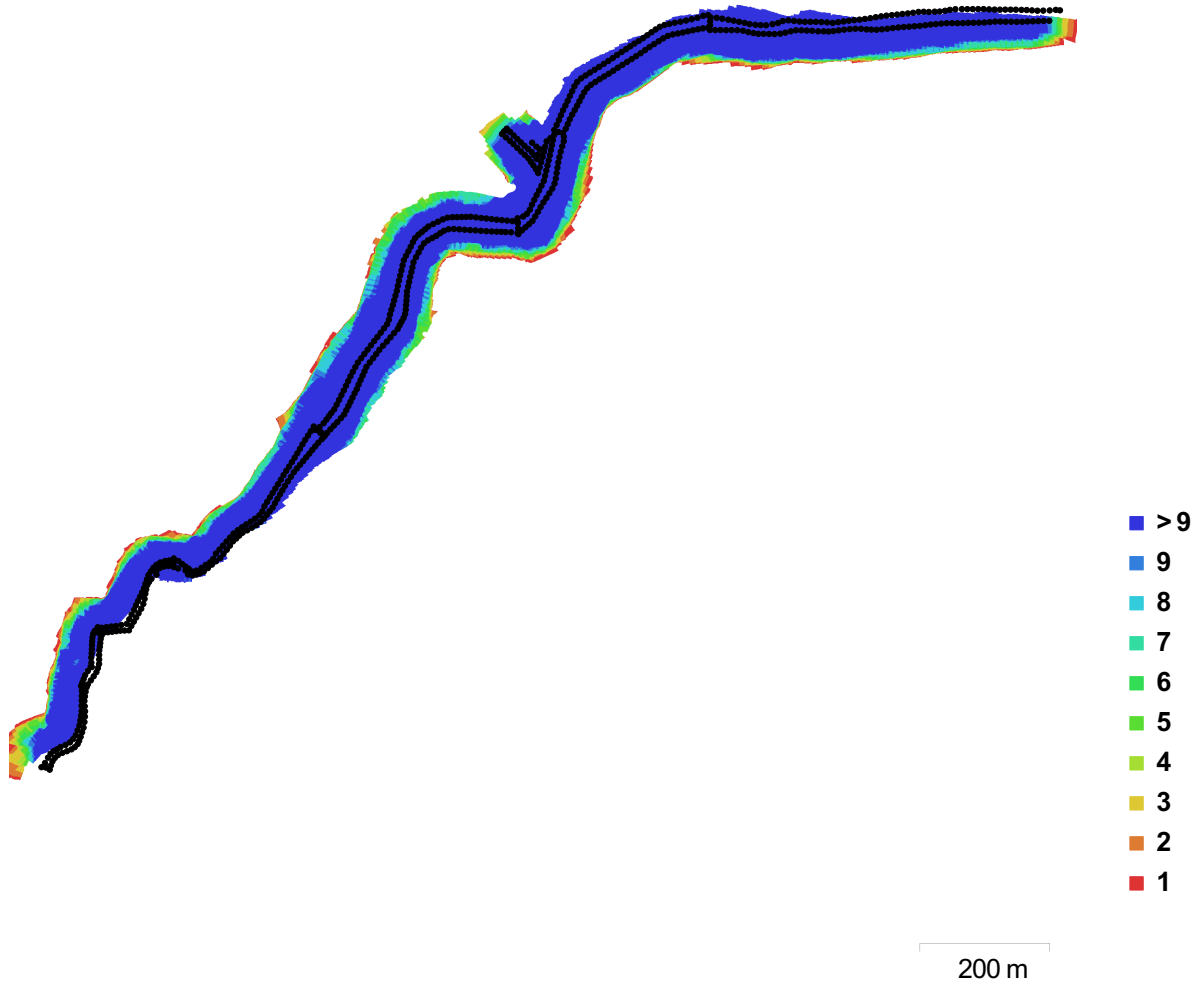


Fig. 1. Camera locations and image overlap.

Number of images:	640	Camera stations:	636
Flying altitude:	66.9 m	Tie points:	356,849
Ground resolution:	1.49 cm/pix	Projections:	2,120,576
Coverage area:	0.183 km ²	Reprojection error:	0.857 pix

Camera Model	Resolution	Focal Length	Pixel Size	Precalibrated
NEX-7 (16 mm)	6000 x 4000	16 mm	4 x 4 μm	No

Table 1. Cameras.

Camera Calibration

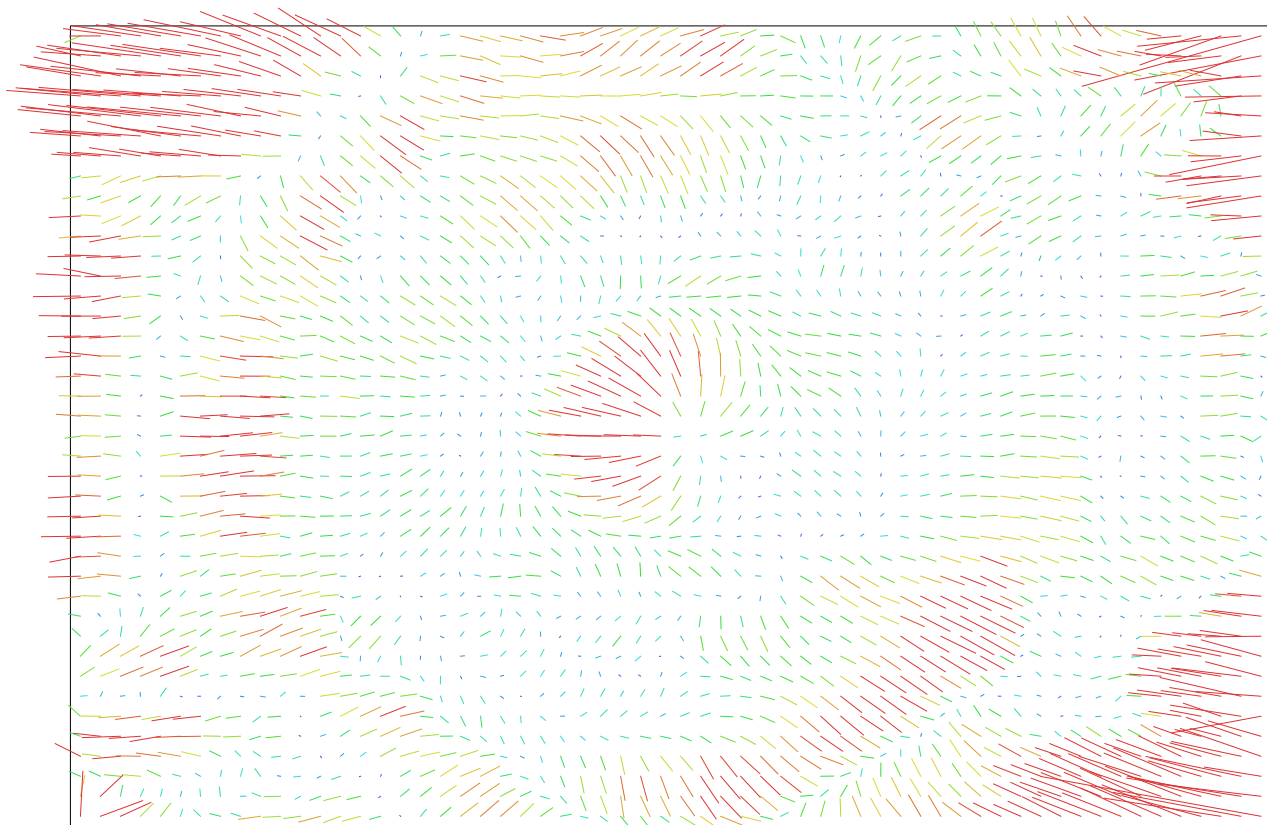


Fig. 2. Image residuals for NEX-7 (16 mm).

1 pix

NEX-7 (16 mm)

640 images

Resolution	Focal Length	Pixel Size	Precalibrated
6000 x 4000	16 mm	4 x 4 μm	No
Type:	Frame	F:	4102.65
Cx:	-22.7474	B1:	1.76775
Cy:	-16.9993	B2:	0.0263453
K1:	-0.00636214	P1:	0.000428398
K2:	0.0109704	P2:	8.59099e-06
K3:	-0.00745138	P3:	0
K4:	0	P4:	0

Ground Control Points

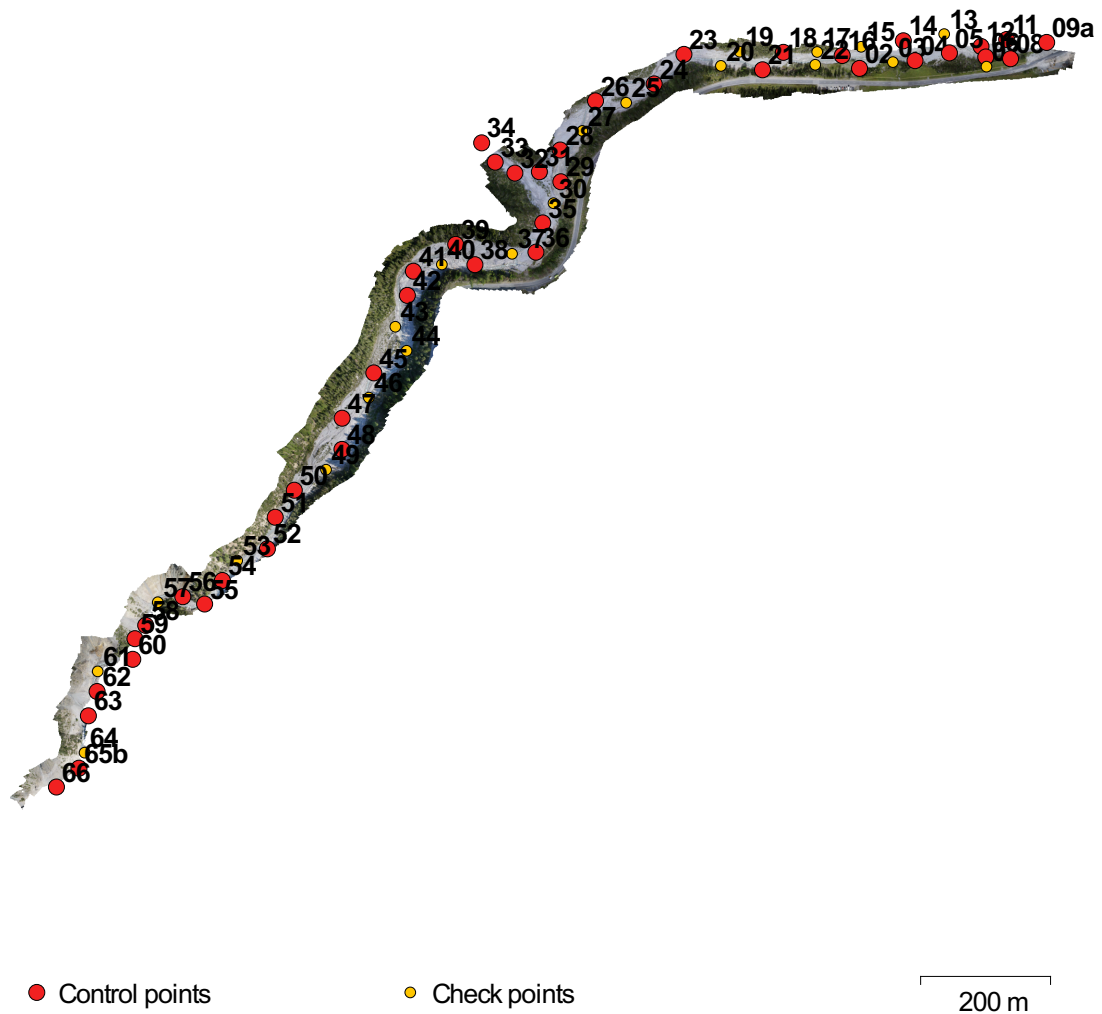


Fig. 3. GCP locations.

Count	X error (cm)	Y error (cm)	Z error (cm)	XY error (cm)	Total (cm)	Image (pix)
42	2.17859	3.95198	2.8771	4.51269	5.35183	0.607

Table 2. Control points RMSE.

Count	X error (cm)	Y error (cm)	Z error (cm)	XY error (cm)	Total (cm)	Image (pix)
21	2.00243	3.21551	3.73876	3.78803	5.32236	0.635

Table 3. Check points RMSE.

Label	X error (cm)	Y error (cm)	Z error (cm)	Total (cm)	Image (pix)
11	0.630878	-1.96744	-2.84841	3.51885	0.535 (13)
12	-0.515248	-3.59713	3.89882	5.32969	0.613 (13)
14	1.95124	-2.23298	1.59918	3.36911	0.532 (15)
16	0.0284112	-5.91504	-2.18266	6.30496	0.434 (16)
18	0.319196	-0.346873	-1.40482	1.4818	0.510 (17)
02	-4.42999	-3.3827	1.50754	5.77409	0.558 (16)
21	0.0675164	2.1054	2.83613	3.53283	0.398 (14)
23	0.177921	-0.38952	-2.9548	2.98567	0.622 (16)
24	0.531751	-2.05784	2.92588	3.61638	0.469 (15)
26	0.19467	1.73322	-0.686751	1.87445	0.735 (12)
28	-0.953789	0.601988	-2.22812	2.49733	0.524 (15)
29	-0.00727354	-1.61699	-1.05991	1.93342	0.548 (35)
31	0.193961	-0.233924	3.27055	3.28463	0.623 (19)
32	-1.94718	-1.3289	-0.370023	2.3863	0.730 (9)
33	2.03427	-1.28986	10.7063	10.9739	0.415 (2)
34					(0)
35	0.591646	-1.27504	2.08453	2.51417	0.887 (15)
36	0.459214	0.82479	-0.491302	1.06421	0.919 (18)
38	2.17406	0.825742	-4.86417	5.39153	0.411 (13)
39	0.913895	1.59709	2.12408	2.81026	0.674 (12)
04	8.11939	21.5499	0.637021	23.0376	0.559 (16)
41	-2.21698	1.10354	-1.98316	3.17266	0.832 (14)
42	-1.74426	0.89722	2.35034	3.06129	0.614 (16)
45	-0.704213	-1.16121	1.09299	1.74326	0.687 (17)
47	1.88408	-0.596891	-0.98006	2.20602	0.637 (21)
48	0.263838	1.69125	-0.745066	1.86683	0.466 (23)
05	-4.43067	-7.13787	-4.3063	9.44056	0.655 (14)
50	1.08783	0.0285585	0.983054	1.46649	0.539 (16)
51	0.662418	0.00659853	-1.86521	1.97936	0.368 (16)
52	-0.557759	-0.360026	1.4301	1.57667	0.505 (15)
54	-1.53144	0.598637	-0.338197	1.6787	0.637 (16)
55	-2.27044	0.226846	1.77685	2.89198	0.499 (17)

Label	X error (cm)	Y error (cm)	Z error (cm)	Total (cm)	Image (pix)
56	2.86408	-0.216483	-0.827903	2.98919	0.603 (25)
58	-1.08483	2.82572	-5.04723	5.88524	0.658 (16)
59	2.00368	-3.47277	2.58603	4.771	0.559 (22)
06	-3.36207	-1.72164	-2.73438	4.66309	0.617 (13)
60	0.976301	-1.83186	0.0419404	2.07621	0.702 (19)
62	-1.70196	1.98122	0.659467	2.69384	0.535 (21)
63	-3.78472	0.521484	3.88889	5.45156	0.612 (19)
65b	1.84476	-1.46149	-0.118965	2.35654	0.804 (20)
66	1.64127	0.78991	-2.66386	3.22705	0.593 (16)
08	1.86765	0.905303	4.32984	4.80158	0.576 (12)
09a	0.51907	2.66982	-0.220689	2.72875	0.464 (9)
Total	2.17859	3.95198	2.8771	5.35183	0.607

Table 4. Control points.

Label	X error (cm)	Y error (cm)	Z error (cm)	Total (cm)	Image (pix)
13	-2.88101	-5.21084	1.47119	6.13331	0.623 (14)
15	-0.938576	-5.44889	-3.61181	6.60428	0.570 (16)
17	-0.414097	-3.4452	-5.3187	6.35055	0.542 (16)
19	2.52961	-2.15326	-7.15503	7.8886	0.512 (19)
20	1.57799	0.301082	-3.79254	4.11874	0.575 (17)
22	1.29653	-1.86157	-2.50278	3.37791	0.466 (15)
25	-1.1361	1.14206	3.40605	3.76779	0.464 (16)
27	0.383609	-0.303505	0.567793	0.74944	0.934 (15)
03	-5.25381	-9.48566	-0.203059	10.8453	0.585 (16)
30	0.876202	-1.9436	-1.5637	2.64395	0.549 (28)
37	0.735443	-0.974093	8.15364	8.24448	0.642 (24)
40	0.723734	2.80768	1.68897	3.35551	0.902 (17)
43	1.30393	0.40212	-2.47188	2.82349	0.710 (19)
44	0.373322	-1.37176	-4.3605	4.5864	0.730 (17)
46	-1.37719	1.42566	1.49882	2.48508	0.509 (18)
49	1.19832	-0.543565	4.66125	4.84341	0.608 (24)
53	-3.32315	0.172378	-0.917771	3.45186	0.477 (14)
57	3.63389	-0.0250547	-4.8629	6.07072	0.883 (27)

Label	X error (cm)	Y error (cm)	Z error (cm)	Total (cm)	Image (pix)
61	-1.0851	1.63184	3.48812	4.00092	0.486 (22)
64	-0.748217	-0.974788	-2.80096	3.05866	0.578 (21)
07	-1.50023	-5.31275	-0.927395	5.59786	0.591 (13)
Total	2.00243	3.21551	3.73876	5.32236	0.635

Table 5. Check points.

Digital Elevation Model



Fig. 4. Reconstructed digital elevation model.

Resolution: 2.97 cm/pix
Point density: 1.13e+03 points/m²

Processing Parameters

General

Cameras	640
Aligned cameras	636
Markers	64
Coordinate system	CH1903+ / LV95 (EPSG::2056)

Point Cloud

Points	356,849 of 422,322
RMS reprojection error	0.323519 (0.857194 pix)
Max reprojection error	2.11155 (37.1003 pix)
Mean key point size	2.62876 pix
Effective overlap	6.43634

Alignment parameters

Accuracy	Highest
Pair preselection	Reference
Keypoint limit	40,000
Tie point limit	4,000
Constrain features by mask	No
Adaptive camera model fitting	Yes
Matching time	1 hours 39 minutes
Alignment time	7 minutes 2 seconds

Optimization parameters

Parameters	f, b1, b2, cx, cy, k1-k3, p1, p2
Optimization time	17 seconds

Depth Maps

Count	636
-------	-----

Reconstruction parameters

Quality	High
Filtering mode	Mld
Processing time	11 hours 26 minutes

Dense Point Cloud

Points	364,185,725
--------	-------------

Reconstruction parameters

Quality	High
Depth filtering	Mld
Depth maps generation time	11 hours 26 minutes
Dense cloud generation time	6 hours 22 minutes

DEM

Size	74,132 x 67,957
Coordinate system	CH1903+ / LV95 (EPSG::2056)

Reconstruction parameters

Source data	Dense cloud
Interpolation	Enabled
Processing time	57 minutes 4 seconds

Orthomosaic

Size	110,530 x 85,788
Coordinate system	CH1903+ / LV95 (EPSG::2056)
Channels	3, uint8
Blending mode	Mosaic

Reconstruction parameters

Surface	DEM
Enable color correction	No
Processing time	25 minutes 7 seconds

Software

Version	1.2.6 build 2834
Platform	Windows 64 bit

Declaration of academic honesty

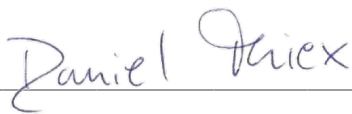
Hereby, I, Daniel Thiex (Student number: 4095529) declare that I have composed the presented master thesis with the title:

Structure from Motion in an alpine environment – evaluation of the method and assessment of channel topography change on the example of the mountain stream Ova dal Fuorn (Swiss National Park (SNP))

independently on my own and without any other resources than the ones indicated. All thoughts taken directly or indirectly from external sources are properly denoted as such.

Tübingen, May 2019

Place, Date



Signature